In vitro characterisation of cell-level neurophysiological diversity in the rostral nucleus reuniens of adult mice

D.A. Walsh[1], J.T. Brown[1] and A.D. Randall[1,2]

[1]Institute of Biomedical and Clinical Sciences, University of Exeter Medical School, Hatherly Laboratory, Exeter, EX4 4PS. [2]School of Clinical Sciences, University of Bristol, Bristol, BS8 1TD.

Key Points

- The nucleus reuniens (Re), a nucleus of the midline thalamus, is part of a cognitive network including the hippocampus and the medial prefrontal cortex. To date very few studies have examined the electrophysiological properties of Re neurons at a cellular level.
- The majority of Re neurons exhibit spontaneous action potential firing at rest. This is independent of classical amino-acid mediated synaptic transmission. When driven by various forms of depolarizing current stimulus Re neurons display considerable diversity in their firing patterns. Due to the presence of a low threshold Ca^{2+} channel, spike output functions are strongly modulated by the prestimulus membrane potential.
- Finally we describe a novel form of activity-dependant intrinsic plasticity which eliminates the high-frequency burst firing present in many Re neurons.
- These results provide a comprehensive summary of the intrinsic electrophysiological properties of Re neurons allowing us to better consider the role of the Re in cognitive processes.

Running title: Cellular neurophysiology of the nucleus reuniens

Abstract

The nucleus reuniens (Re) is the largest of the midline thalamic nuclei. We have performed a detailed neurophysiological characterization of neurons in the rostral Re of brain slices prepared from adult male mice. At resting potential (-63.7 ± 0.6 mV), circa 90% of Re neurons fired action potentials, typically continuously at ~8 Hz. Although Re neurons experience a significant spontaneous barrage of fast, amino-acid-mediate synaptic transmission, this was not predominantly responsible for spontaneous spiking as firing persisted in the presence of glutamate and GABA receptor antagonists. With resting potential preset to -80 mV -20 pA current injections revealed a mean input resistance of 615 MΩ and mean time constant of 38 ms. Following cessation of this stimulus a significant

rebound potential was seen that was sometimes large enough to trigger a short burst of very high frequency (100-300 Hz) firing. In most cells short (2 ms), strong (2 nA) current injections elicited a single spike followed by a large afterdepolarizing potential (ADP) which, when suprathreshold, generated high frequency spiking. Similarly, in the majority of cells preset at -80 mV, 500 ms depolarizing current injections to cells led to a brief initial burst of very high frequency firing, although this was lost when cells were preset at -72 mV. Biophysical and pharmacological experiments indicate a prominent role for T-type Ca^{2+} channels in the high-frequency bursting of Re neurons. Finally, we describe a novel form of activity-dependent intrinsic plasticity that persistently eliminates the burst firing potential of Re neurons.

Abbreviations. ADP, after-depolarization potential; αEPSC, EPSC like waveform; AHP, afterhyperpolarization; AP, action potential; HCN, hyperpolarisation-activated cyclic nucleotide gated; HPC, hippocampus; mPFC, medial prefrontal cortex; Re, nucleus reuniens; TTX, tetrodotoxin;

Introduction

The nucleus reuniens (Re) is the largest of the midline thalamic nuclei. Located within the interthalamic adhesion, Re is a component of the higher-order thalamus, a group of thalamic structures which receive little sensory input. Instead, such areas form extensive cortico-thalamo-cortical pathways (Vertes et al 2015). The roles of Re have been the subject of growing interest in recent years (Cassel *et al.*, 2013; Aggleton, 2014). In rodents, experimentally-induced lesions to Re result in a range of cognitive outcomes (Xu & Südhof, 2013; Cholvin *et al.*, 2013; Hallock *et al.*, 2013); whereas in man this brain area is selectively compromised in Korsakoff's syndrome (amnesic-confabulatory syndrome), a form of dementia resulting from thiamine (vitamin B1) deficiency- often arising from alcoholism or malnutrition, but also associated with eating disorders, chemotherapy or persistent vomiting such as that in hyperemesis gravidarum (Mair *et al.*, 1979).

The contributions of Re to cognitive function have a sound grounding in its neural connectivity (Cassel *et al.*, 2013; Aggleton, 2014). In particular, Re output is almost exclusively directed to the hippocampus (HPC) and limbic cortex. This includes strong monosynaptic projections to structures with key roles in cognitive function– notably area CA1 and the subiculum of (particularly ventral) HPC and much of the medial prefrontal cortex (mPFC) (Vertes, 2006; Vertes *et al.*, 2007, 2015; Prasad & Chudasama, 2013; Varela *et al.*, 2014). This wiring allows the Re to "close a synaptic loop" between the ventral hippocampus (HPC)/subiculum and the mPFC. Indeed, afferents from the mPFC have been demonstrated to synapse on Re neurones that in turn project to CA1 (Vertes *et al.*, 2007) .

Functionally speaking, Re innervation of the hippocampus appears to be substantial. It is reported, for example, that electrical stimulation of the Re *in vivo* produces substantial, monosynaptic latency, excitatory responses in neurons of hippocampal area CA1 (Dolleman-Van der Weel *et al.*, 1997). Excitation of both pyramidal cells and interneurones is reported (Dolleman-Van der Weel *et al.*, 1997; Dolleman-Van der Weel & Witter, 2000). Interestingly, Re stimulation is reported to be as effective in discharging hippocampal CA1 pyramidal cells as equivalent stimulation of hippocampal area CA3, the presynaptic source of the intensively studied Schaffer collateral commissural pathway. Furthermore, Re-CA1 synapses exhibit greater frequency facilitation than CA3-CA1 connections, and at least as much long-term potentiation (Bertram & Zhang, 1999). The synapses responsible for this robust synaptic drive are predominantly located within *stratum lacunosum moleculare,* where the distal dendrites of CA1 cells are found as well as the temporo-ammonic axons that conveying direct excitatory input from the entorhinal cortex. Indeed, it is likely that investigators using

extracellular electrical stimulation of hippocampal slices in attempts to drive the temporoamonic input to CA1 cells (Giocomo & Hasselmo, 2006; Ceolin *et al.*, 2011; Booth *et al.*, 2016*b*) are additionally recruiting Re axons. Interestingly, *in vivo* awake tetrode recording has recently revealed that Re has “head direction” cells (Jankowski *et al.*, 2014), a neural activity more commonly associated with neurons in the entorhinal cortex and hippocampus/subiculum (Taube *et al.*, 1990; Sargolini *et al.*, 2006). This finding prompted further investigation of spatially responsive cells in the Re which revealed evidence of both place cells and border cells, providing further evidence for the importance of the Re in spatial navigation (Jankowski *et al.*, 2015).

In vivo recordings have also demonstrated the presence of Re neurons which exhibit trajectory-dependant firing during a T-maze based continuous alteration task, similar to neural activity observed in the CA1 region of the hippocampus and the mPFC. Interestingly, lesioning or optogenetic silencing of the Re leads to a substantial reduction in trajectory-dependant firing in CA1. This suggests that the Re plays an important role in the transfer of information from the mPFC to CA1 that pertains to future path choices in goal-directed behaviours (Ito *et al.*, 2015). Another recent in vivo study (Hallock *et al.*, 2016) has also indicated that structures in the midline thalamus are crucial for the synchronous oscillatory behaviour that arises between the hippocampus and pre-frontal cortex during working memory tasks (Jones & Wilson, 2005).

Despite the significant body of data that address the connectivity of the Re, its roles in behaviour, and its pathology in disease, neurophysiological understanding of this cognitively important thalamic structure is far from comprehensive. Practically all published Re neurophysiology to date has been performed with *in vivo* extracellular recording methods either in anesthetized (Dolleman-van der Well 1997, Bertram and Zhang 1999) or, more recently, awake behaving rats (Jankowski *et al.*, 2014; Ito *et al.*, 2015; Hallock *et al.*, 2016). Unquestionably there have been few detailed cell-level electrophysiological studies of Re neurons. Working in the mid-line thalamus, which likely included Re, Graef and colleagues examined changes to bursting and T-type Ca^{2+} channels produced in a pilocarpine-induced epilepsy model (Graef *et al.*, 2009). The same group subsequently made a similar study, in this case specifically working within Re, examining consequences of ethanol exposure and withdrawal (Graef *et al.*, 2011). The only other intracellular data from Re neurons we are aware of are a single panel in a supplementary figure in Xu and Sudhof 2013- which presents miniature IPSCs recorded from 6 mice at 26ºC.

Given the growing interest in the neural functionality of Re we have embarked upon a series of *in vitro* brain slices studies designed to better characterize the cellular neurophysiology of

Re. We outline the intrinsic excitability properties of neurons in the rostral Re, studies entirely performed using coronal brain slices prepared from adult male mice.

Methods

Ethical approval

All work in this study was approved by the University of Exeter Animal Welfare Ethical Review Board. Animals were sacrificed in accordance with schedule 1 of the UK Animals (Scientific Procedures) Act 1986 and the subsequent amendments regulations of 2012, as implemented in response to directive 2010/63/EU of the European Parliament and of the Council on the protection of animals used for scientific purposes.

Animals and tissue preparation

All tissues for this study were obtained from male C57-Bl/6 mice bred in the University of Exeter Biological Services Unit using founders purchased from Charles River. All animals were granted *ad libitum* access to both food and water and were housed on a 12/12 light dark cycle. For this study, all animals were aged 16-18 weeks and were sacrificed by cervical dislocation. The brain was rapidly removed and placed an in ice-cold slicing medium consisting of (in mM): 189 Sucrose, 10 D-Glucose, 26 $NaHCO_3$, 3 KCl, 5 $Mg_2SO_4(7H_2O)$, 0.1 $CaCl_2$, 1.25 NaH_2PO_4. Serial 300 μm thick coronal sections were then prepared using a Leica VT1200 vibratome. Following preparation, slices were allowed to recover for at least 1 hour at room temperature in our standard recording aCSF. This was composed of (in mM):124 NaCl, 3 KCl, 24 $NaHCO_3$, 1.25 NaH_2PO_4, 2 $CaCl_2$, 1 $MgSO_4(7H_2O)$, 10 D-Glucose, and was gassed with carbogen (i.e. 95% O_2 /5% CO_2)

Only one slice, containing a suitable section of rostral Re could be obtained per mouse. This was centred at approximately Bregma -0.46 to -0.58. The required slice was identified with the aid of the Paxinos and Franklin mouse brain atlas. In coronal slices at this level the location of Re can be readily pinpointed as a bi-lobed structure lying atop the third ventricle. We never use slices that had been previously treated with any drug for subsequent electrophysiological recordings, this has limited the amount of pharmacological data that we have been able to gather from Re, as at most one pharmacological intervention can be studied per animal.

Electrophysiological Recordings

All recordings were made using the patch clamp technique. The slice containing the rostral Re was transferred into a submerged recording chamber which was perfused with gassed aCSF and maintained at a temperature of ~33˚C. The recording chamber was mounted on the stage of an upright microscope (Olympus BX51) and cells were visualised using infrared differential interference contrast optics and a CMOS USB 2.0 camera (Thor Labs). Drug applications were made by addition to the perfusing aCSF.

Microelectrodes of 3-5 MΩ resistance were fabricated from borosilicate glass capillaries using a P-97 Flaming Browning micropipette puller. Pipettes were filled with a K-Gluconate based internal solution composed of (in mM): 130 K-Gluconate, 20 KCl, 10 HEPES free acid, 0.2 EGTA, 0.3 GTP-Na salt, ATP-Mg salt, pH adjusted to 7.3 with KOH. The 15 mV junction potential error that arises from the pairing this pipette solution with our aCSF was corrected for during analysis.

Cells of the rostral Re were visually identified based on their location relative to the dorsal tip of the third ventricle. All recordings were made with a Multiclamp 700B amplifier (Molecular Devices) and digitised with a Digidata 1440A interface (Molecular Devices). All data were stored on a personal computer (Hewlett-Packard) using pClamp 10.4 software. This package was also used to design and deliver the various experimental protocols employed to characterize the cells.

Data Analysis

Data were analysed using a range of custom written MATLAB scripts and pClamp 10.4 software. Statistical assessments of differences between populations were made using unpaired two-tailed students t-tests and both one and two way analysis of variance (ANOVA) as appropriate. Figures were prepared with Origin 9.1.

Results

Cellular properties at resting potential

Data collected from intact Re neurons using loose patch/cell-attached recording indicated that the majority of cells exhibited a significant degree of spontaneous action potential (AP) firing. Figure 1A(a) illustrates a segment of such activity from a typical recording of this nature. The timecourse of the instantaneous frequency of action potential firing for this cell recorded over 60 s is presented in Figure 1A(b).

Commensurate with observations made in loose-patch or cell-attached mode (Figure 1A), robust spontaneous AP firing was also observed in the majority of Re neurons when we entered the whole cell recording mode and immediately collected a 60 s period of current clamp data with zero injected current (i.e. recording at resting potential). In 135 of 154 (~88%) whole cell recordings of this nature, the neuron fired one or more spontaneous APs during the 60 s epoch immediately following entry into the whole cell configuration (Figure 1B). For all cells (i.e. both spontaneously firing and silent) the average membrane potential observed over the entire 1 minute period is presented in Figure 1C. The 19 cells exhibiting no spontaneous spiking were characterized by a membrane potential (-70.6 ± 3.2 mV) somewhat more negative than the overall population mean (-63.7 ± 0.6 mV). The vast majority (107) of the 135 cells that exhibited AP firing maintained their spiking activity throughout the entire 60 s period, with no single interspike interval longer than 5 s (and in most cells no longer than 300 ms). These cells had a mean resting potential of -61.4 ± 0.4 mV (n=107). For these recordings a histogram presenting the distribution of mean AP frequency is shown in Figure1D. This was compiled by calculating the average of the reciprocal of all inter-spike intervals for each cell. The average of these mean instantaneous frequencies was 9.2 ± 0.5 Hz.

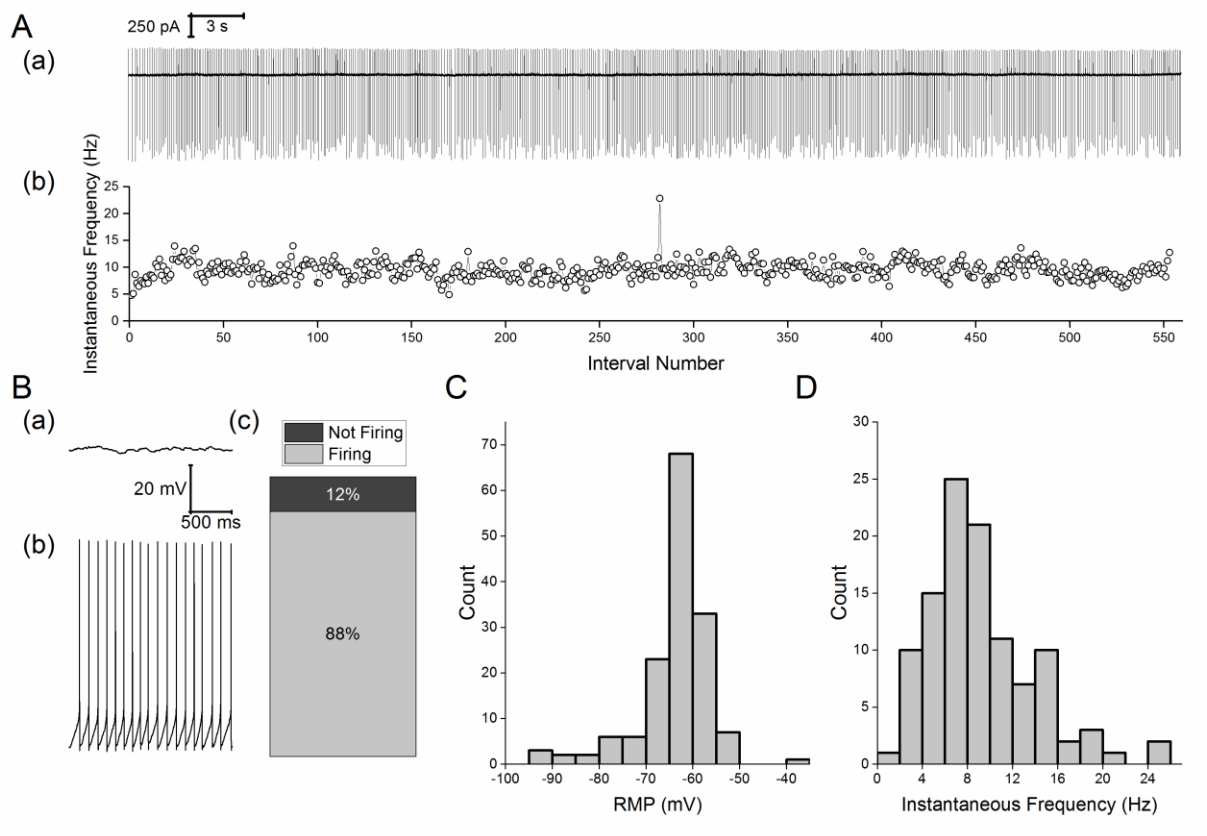

Figure 1. Firing properties at rest. (A) (a) Sample trace of spontaneous AP firing recorded in cell-attached mode over a 60 s period. (b) A plot showing the Instantaneous frequency vs spike interval number for this cell-attached recording. **(B)** Sample traces from whole cell current clamp recordings illustrating (a) a neuron which showed no spontaneous activity and (b) a neuron that fired regularly at rest. (c) A cumulative column representation of the percentage of silent and spontaneously firing neurons in the Re population. **(C)** Histogram presenting the mean resting membrane potential recorded during a 60 s epoch soon after gaining whole cell access **(D)** Histogram showing, for firing cells, the mean instantaneous AP frequency at RMP during this 60 s epoch.

In the remaining 27 cells that fired any AP during the 60 s recording epoch a range of spiking behaviours was observed. In 9 of the cells APs initially fired regularly at 3-10 Hz, essentially in a fashion mirroring the majority group illustrated in Figures 1B and D, but at some stage this activity first slowed and then ceased, seemingly as a consequence of modest and progressive (2-4 mV) hyperpolarizing shift in resting potential (Figure 2A). In the remaining 18 cells in which any spontaneous AP generation was seen prolonged spike-free periods (at least 5 s) were interrupted by brief periods of spiking. These cells fell into two clear groups. The first comprised 12 cells in which the intermittent spiking only comprised low frequency (<15 Hz) activity (Figure 2B), essentially similar to the spiking seen in the cells that maintained their firing for the whole 60 s (Figure 1). The second group comprised only 6 cells (Figure 2C), in these occasional brief bouts of spontaneous firing were observed which included very much briefer inter-spike intervals (as short as 3.2 ms), and thus considerably higher maximum instantaneous frequencies of spiking (75-310 Hz). A noticeable difference between the 11 cells with low frequency intermittent firing and the 6 cells with occasional high frequency bursting was in resting potential. In the latter group this was always more negative than -75 mV (mean -82.2 ± 2.9 mV), whereas in the 11 cells in which the intermittent AP firing comprised only of low frequency spiking the resting potential was significantly more depolarized (-66.0 ± 1.9 mV, $p<0.005$ unpaired t-test). This latter value lies between the average membrane potential of the 17 cells that fired no AP in 60 s (circa -70 mV) and the largest group of cells, those exhibiting maintained regular firing (circa -61 mV). The very negative membrane potential of the 6 cells in high frequency spiking group, meant that the observed bursts rode atop a substantial transient depolarizing shift which brought the cells to threshold, the nature of which will be discussed below.

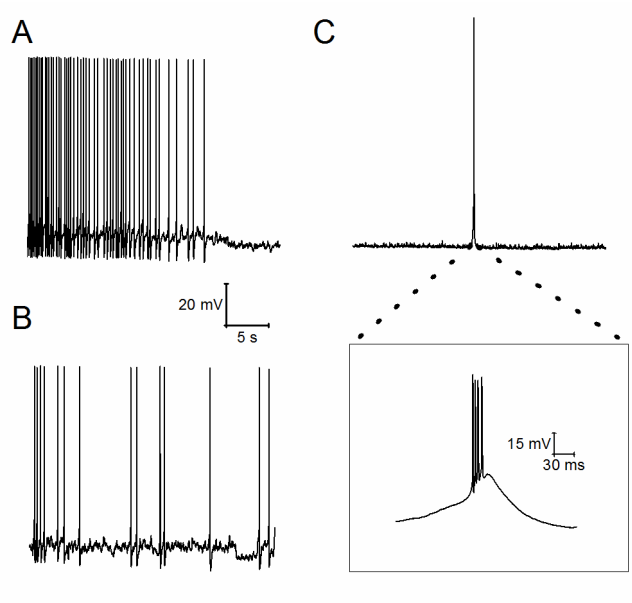

Figure 2. Heterogeneous firing patterns at rest. Sample current clamp trace of **(A)** an initially regularly firing neuron in which cessation of firing was accompanied by a hyperpolarising shift in resting membrane potential, **(B)** a neuron exhibiting irregular firing at a low frequency and **(C)** a neuron which fired irregularly in short high frequency bursts. The inset shows the very high frequency spiking present in such a burst with 4 AP arising in under 30 ms.

As described above, ~70% of Re neurons fired constantly at rest with a frequency of 2-20 Hz (Figure 1D). Inspection of the voltage traces revealed that this firing appeared to be predominantly paced by a robust afterhyperpolarization (AHP) that followed each AP. On average this AHP peaked 13.7 ms after the AP peak and took the membrane potential to -20.1 mV below the previous spike threshold (Figure 3A). As the AHP decayed and the cell depolarized again it was able to initiate another spike; consequently the rate of the AHP decay was appeared to be a key determinant of spontaneous firing frequency.

In the 134 cells firing spontaneously at rest we detected all of the spikes and characterized their core waveform properties. For the 120 cells firing a total of 20 or more AP histograms plotting the distribution of mean AP threshold, max rate of rise, zenith and width at half height (defined as the voltage halfway between AP threshold and zenith) are presented in Figure 3B-E. When the distribution of AP thresholds (Figure 3B) is compared with the resting potential distribution (Figure 1C) it is apparent why most Re neurons exhibit spontaneous firing. As expected, bath application of tetrodotoxin (TTX) (500 nM) first slowed and then eliminated spontaneous AP firing in Re neurons (data not shown)).

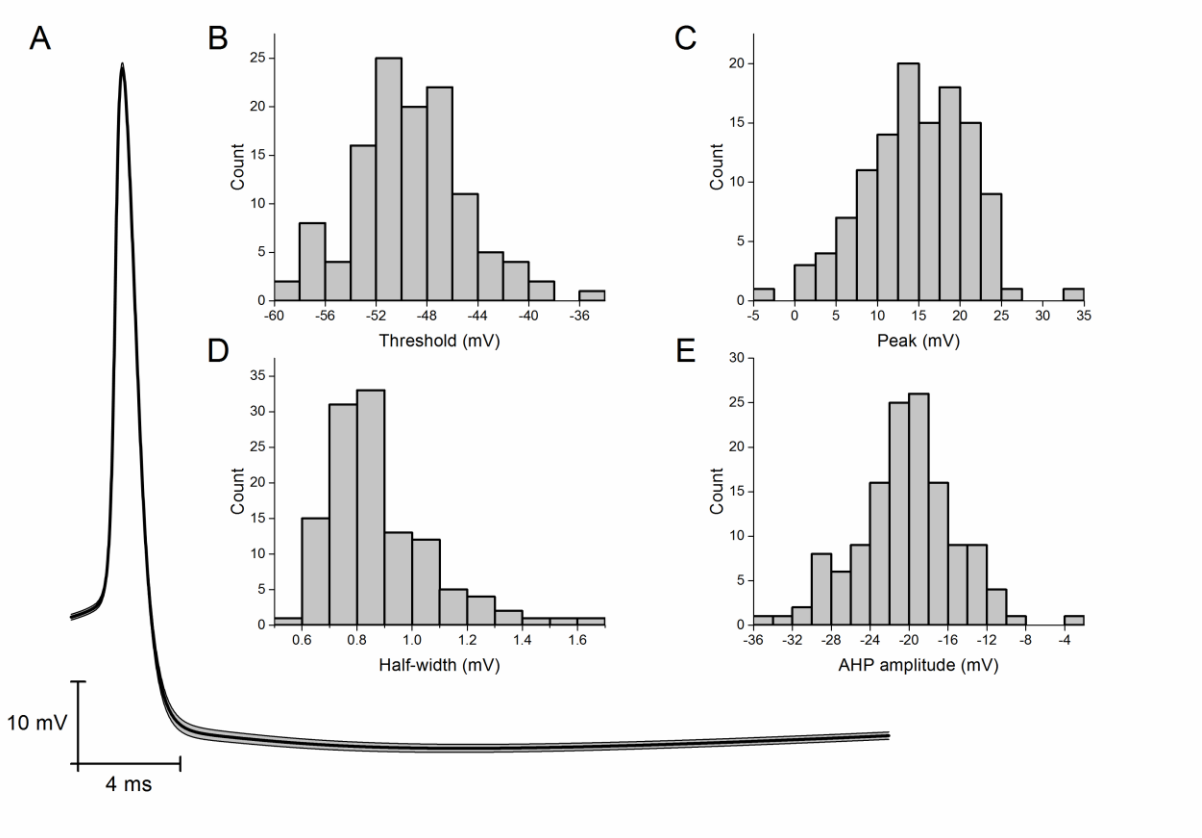

Figure 3. Action potential properties (A) Average trace of a spontaneous action potential measured at RMP. SEM is highlighted in grey. **(B-E)** Histograms showing the average spike properties of spontaneously fired APs, specifically **(B)** AP threshold, **(C)** AP peak value (i.e. zenith), **(D)** AP width measured at half height and **(E)** AHP amplitude.

It was clear from close examination of current clamp recordings at rest that Re cells *in vitro* received a significant degree of spontaneous synaptic input (Figure 4A). Classical fast spontaneous synaptic activity was also apparent in recordings made in voltage clamp mode at a holding potential of -85 mV (Figure 4B). Indeed, spontaneous IPSCs recorded in vitro in voltage clamped Re cells at 26°C have been presented in one previous publication (Xu & Südhof, 2013).

When, during voltage clamp recordings, TTX (500 nM) was added to the perfusing aCSF to isolate miniature inward-going synaptic events (i.e. post-synaptic responses arising from presynaptic release of single quanta), we saw a spread of response amplitudes with a median peak of typically around 10-15 pA. Most of these events rose very fast and decayed rapidly and exponentially with a time constant of around 1 ms (Figure 4C mPSCs).

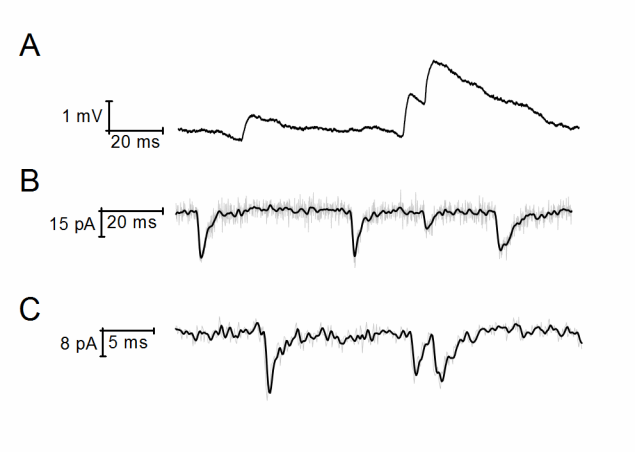

Figure 4. Spontaneous synaptic input. (A) Sample post-synaptic potentials measured at RMP. **(B)** Sample inward going post-synaptic currents measured at a holding potential of -85 mV. **(C)** Sample trace of miniature post-synaptic currents measured at a holding potential of -85 mV in the presence of 500 nM TTX. Black current traces in **(B&C)** are Gaussian filtered versions of the raw grey traces.

We wished to establish if the spontaneous synaptic drive to Re cells could be a major factor in their spontaneous AP firing. We therefore made a series of recordings in the maintained presence of NBQX (5 µM), L689560 (5 µM) and gabazine (5 µM) to block AMPA/Kainate, NMDA and $GABA_A$ receptors, respectively. Under these conditions spontaneous post-synaptic potentials were absent but the mean resting potential remained relatively depolarized (-66.7 ± 2.1 mV, n=29, Figure 5A). Furthermore, spontaneous AP electrogenisis was still apparent in the majority (20/29, 69%) of cells (Figure 5B). This spontaneous activity occurred with a mean frequency of (8.0 ± 1.0 Hz) very similar to that observed in the absence of pharmacological block of amino-acid mediated synaptic transmission (Figure 1D). The various waveform properties of spontaneous action potentials also appeared unaffected by synaptic blockade (data not shown). This indicates that the relatively depolarized resting potentials and consequent tonic spontaneous AP firing in Re neurones *in vitro* arises largely from cell-intrinsic properties, rather than synaptic drive, although the latter will not doubt shape this activity to some extent.

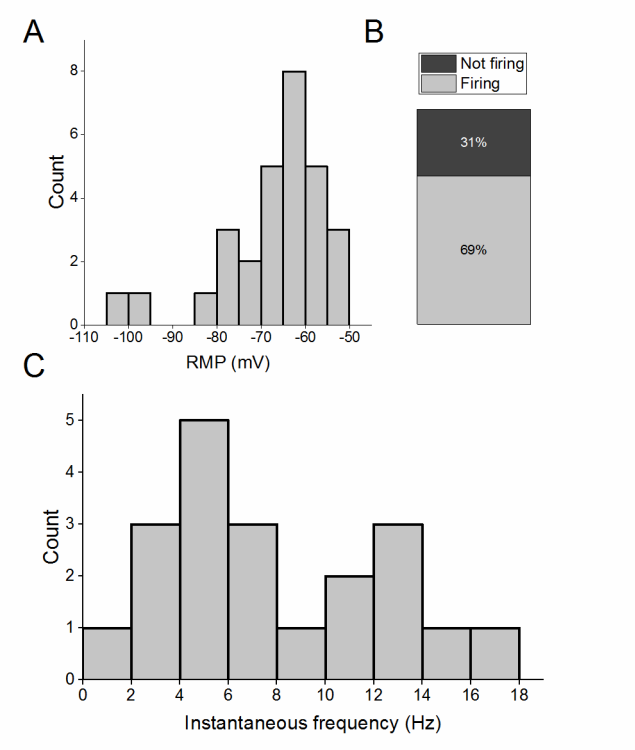

Figure 5. Firing properties at rest in the presence of synaptic blockers. (A) A plot illustrating the distribution of resting membrane potentials in Re cells recorded in the combined presence of blockers of AMPA/Kainate, NMDA and $GABA_A$ receptors, right. **(B)** An illustration of the relative proportions of spontaneously firing and silent cells under these conditions **(C)** The distribution of mean instantaneous AP frequency at RMP during a 60 s epoch recorded in whole cell configuration. All recordings were made in the presence of NBQX (5 µM), Gabazine (5 µM) and L-689560 (5 µM).

Excitability analysis from a defined pre-set membrane potential

For a variety of underpinning biophysical reasons, the intrinsic excitability properties of all neurons depends on their resting membrane potential (see below for data exemplifying this). Consequently, to make comparisons across neurons within a population it is helpful to set the pre-stimulus membrane potential of each cell to constant defined level. Furthermore, it is helpful to choose a pre-stimulus potential at which spontaneous firing is absent, because the presence of ongoing background firing complicates interpretation of any subsequent stimulus-evoked activity. Thus, to gain a detailed insight into the intrinsic excitability of Re neurons we initially chose to make measurements from a pre-stimulus membrane potential of -80 mV. This pre-stimulus potential was set by applying a suitable amount of bias current via the recording amplifier; this varied in amplitude from +46.8 to -153.7 pA, averaging -45.4 pA (n=154).

Having set the pre-stimulus membrane potential to -80 mV, we then applied a range of defined current stimuli to probe the sub- and supra-threshold intrinsic properties. Firstly, to determine an approximation of “rheobase” for cells at -80 mV we applied an incremental series of 100 ms duration, depolarizing current injections. These were increased stepwise in amplitude in small increments at 1 Hz until action potential firing was observed. As illustrated in Figure 6A, cells could be divided into those which fired just one AP at rheobase and those which produce a burst of between 2 and 6 AP. The mean AP count in latter group was 2.9 ± 0.2 AP . Data summarizing the amount of current required to produce at least one AP across 106 cells is shown on the left of Figure 6B. Alongside this are data from an series of similar recordings made in the synaptic blocker cocktail described above. These exhibited an almost identical mean rheobase of 25.3 ± 5.1 pA (n=25, Figure 6B). For the larger drug free experimental group Figure 6C compares the mean rheobases for those cells firing just one AP and those producing a burst of 2-6 AP. The latter group had a 25% lower rheobase (P=0.01, unpaired t-test), and consequently were both easier to bring to AP threshold and once there produced a greater spike output.

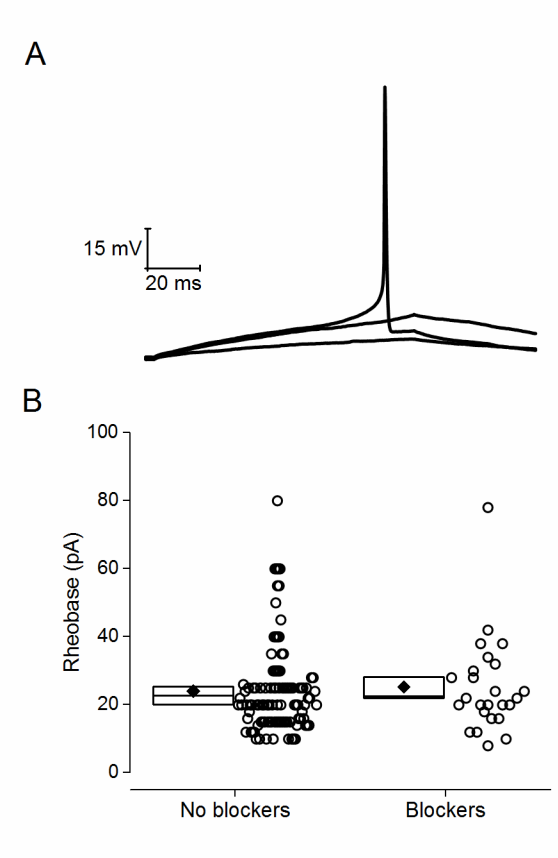

Figure 6. Approximation of rheobase from a pre-stimulus potential of -80 mV. (A) Sample voltage traces extracted from a series of incrementally growing 100 ms current injections used to approximate the rheobase from -80 mV. Data are shown are from 2 cells, one with a single spile and one with a burst. The traces shown in each are responses to the minimal current injection which elicited an AP (rheobase), rheobase – 2 pA and rheobase/2. **(B)** A plot comparing rheobase distributions recorded both in the absence and presence of NBQX (5 µM), Gabazine (5 µM) and L-689560 (5 µM). (C) The "no blocker" data from (B) broken down by cells which fired only one AP at rheobase and cells which generated a burst of 2-6 AP, data are treated . In (B) and (C) each round symbol is a separate recording. The diamonds plot the mean, the boxes the standard error and the line crossing the box the median. We next employed a standard incremental current injection protocol in which a series of 9 consecutive 500 ms current stimuli were delivered with an inter-stimulus interval of 10 s. The amplitude of the first current pulse was -20 pA and each subsequent pulse was +10 pA larger such that the final pulse had an amplitude of +60 pA (Figure 7A)). The first (i.e.-20 pA stimulus) sweep was used to determine the subthreshold intrinsic properties of Re neurons including input resistance, membrane time constant, and capacitance. Approximately 12% of Re cells exhibited a significant rebound depolarization following cessation of hyperpolarizing current injections. As reported previously by others (Graef 2011) these rebound depolarizations were capable of driving spiking in some cells (Figure 7B), and when spiking was seen multiple AP were typically produced within a short time window. The basis of this rebound potential will be described later.

Input resistance averaged 615 ± 17 MΩ (Figure 7D), and mean membrane time constant was 38.5 ± 1.1 ms (Figure 7E). The capacitance estimated by dividing time constant by input resistance averaged 66.6 pF, indicating that, for CNS neurons, these cells were modest in size.

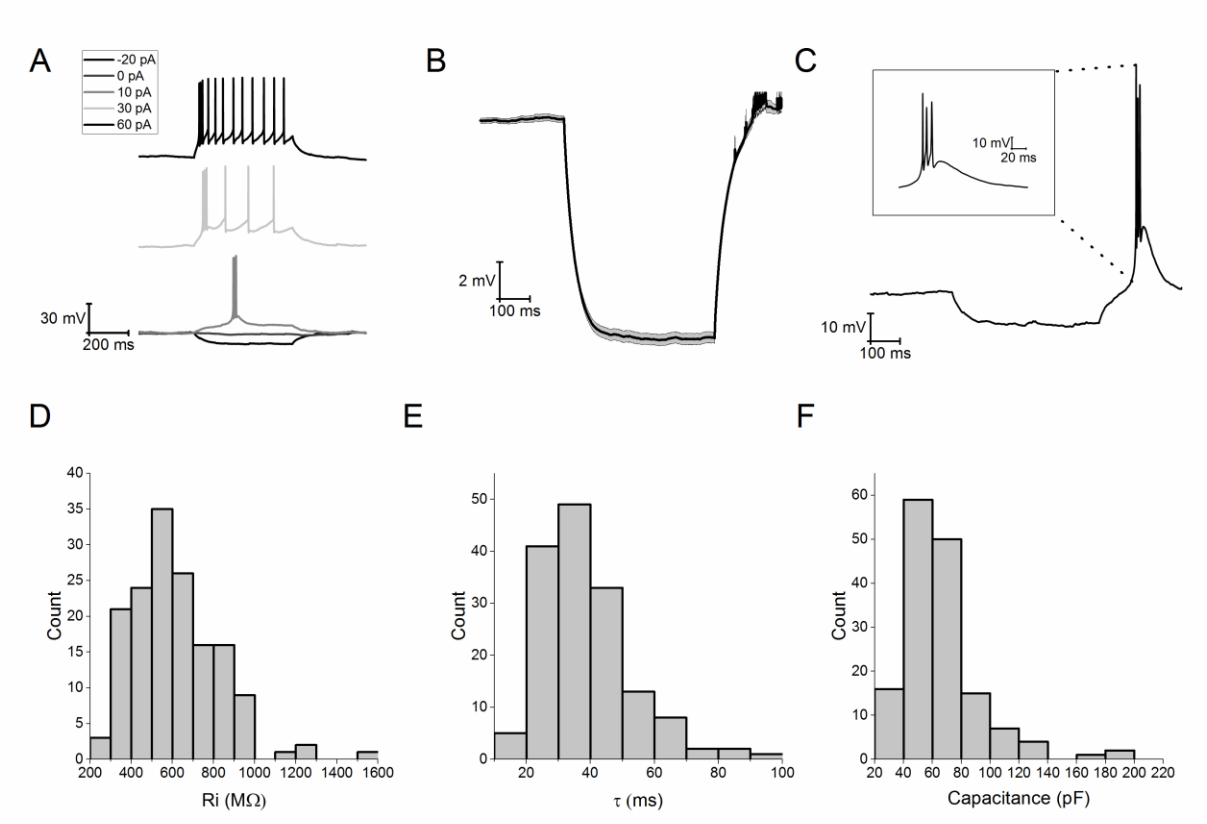

Figure 7. Passive membrane properties. (A) Sample voltage traces a series of current injections (-20 – 60 pA) from a set pre-stimulus potential of -80 mV. For clarity the responses to 30 and 60 pA stimuli have been offset. **(B)** Average voltage response to a -20 pA, 500 ms hyperpolarising current injection from a set pre-stimulus potential of -80 mV. SEM is highlighted in grey. Highlighted in **(C)** is the high frequency rebound spiking behaviour observed from some cells following termination of negative current injections. **(D-F)** Histograms showing **(D)** input resistance, **(E)** time constant and **(F)** an approximation of capacitance.

A slow depolarizing relaxation of the membrane potential and accompanying decrease in membrane resistance during application of a hyperpolarizing current injection is commonly known as ”sag”. It is a prominent and important subthreshold feature of a number of CNS neurons, and arises from activation of hyperpolarisation-activated cyclic nucleotide gated (HCN) channels. The majority of Re neurons exhibited little or no sag in response to a 500 ms, 20 pA hyperpolarising current injection, as exemplified by the average voltage traces shown inFigure 7B. The extent to which HCN2 channels, the predominantly expressed HCN channel in the thalamus (Santoro *et al.*, 2000), would activate in response to a relatively short hyperpolarising current injection is questionable given this channels long activation time constant (in the order of seconds). However when we employed a five fold longer 20 pA hyperpolarising step (2.5 s) we also observed no appreciable sag as exemplified by the

average trace in Figure 8A. In case HCN channels were already largely activated at -80 mV we also examined 2.5 s 20 pA current injections at -72 mV and 500 ms current injections at -64 mV, neither of which exhibited any significant sag.

To finally confirm this apparent paucity of HCN current, and to look for any potential activation from even more depolarized prestimulus potentials, we also carried out a series of voltage-clamp recordings to look for any sign of HCN-like conductances. Here we applied a series of 5 s duration hyperpolarising steps to Re cells at a holding potential of -55 mV. The test potential varied from -60 to -125 mV in 5 mV increments (Fig 8B). In such protocols HCN channel activity is revealed by a slowly growing inward current that takes 10s or 100s of milliseconds to come to steady state level. The cross-cell average current response from 6 Re neurons can be seen in Figure 8A. In this average there is no sign of any slow gating HCN-like current. The presence of HCN currents can be readily revealed by looking for difference between the current level in the first few milliseconds following hyperpolarization (before the slowly gating HCN channels have opened) and that seen at the end of the voltage pulse (when the HCN channel opening probability has had time grow). Such an analysis in presented in Figure 8C. This compares of the inward current level recorded in the first and last 60 ms of the voltage step to -125 mV relative to the holding current. This revealed that 5 of the 6 neurons recorded exhibited no slow gating inward current whatsoever. The remaining neuron exhibited a small (~50 pA) growth in inward current although on average, across the 6 cells, there was no significant difference in current level at the start and end of the pulse (Fig 8C). Upon inspection of the average voltage trace (Fig 8B) it became clear that the amplitude grew in a non-linear fashion across sequential voltage steps. This is also evident from Figure 8D, an I-V plot of the current amplitude at the end of the 5 s step versus voltage. This form of this curve is suggestive of the presence of inwardly rectifying potassium channels as the membrane conductance increases at potentials negative to the potassium equilibrium potential.

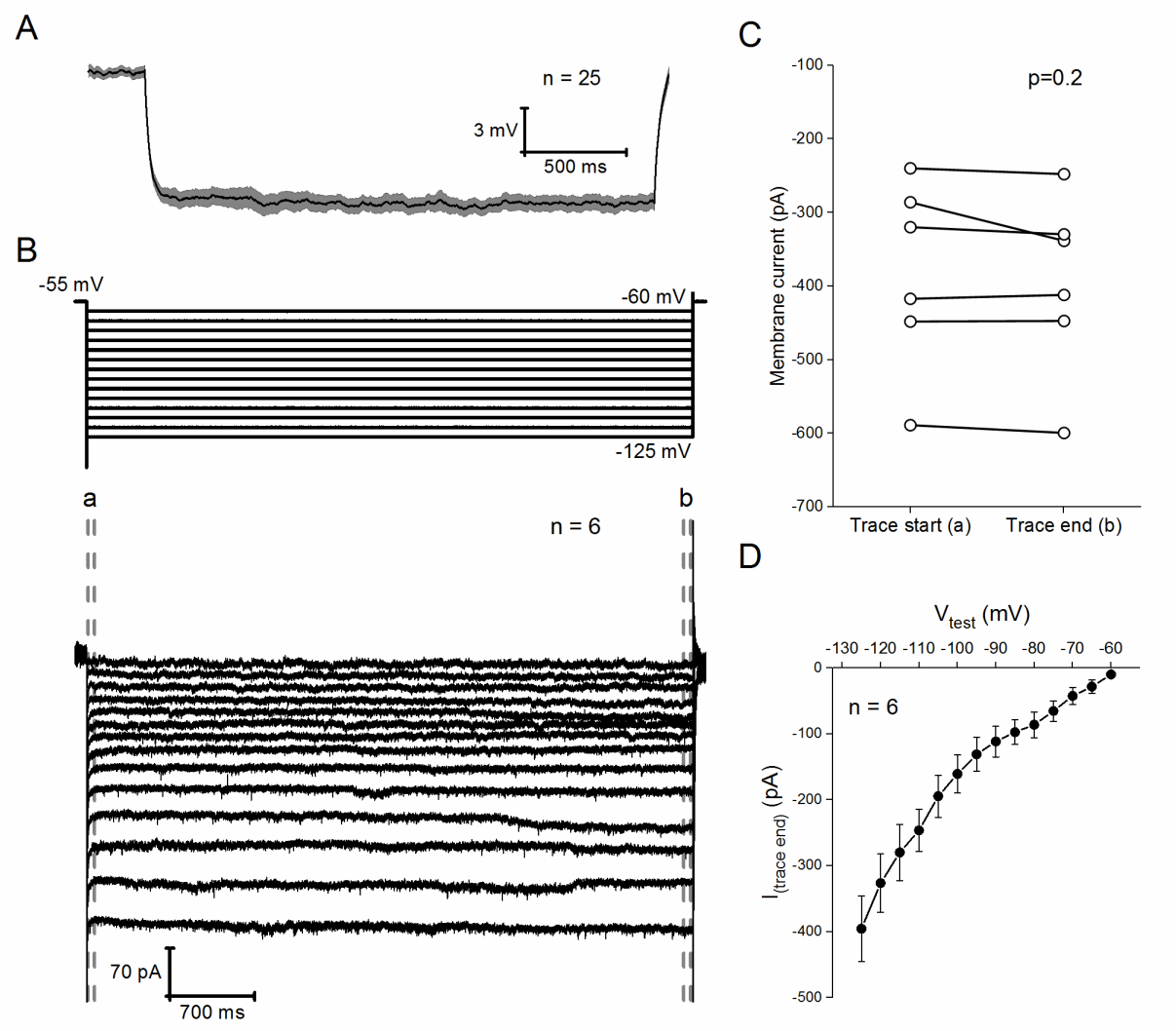

Figure 8. Absence of HCN channel-like current. (A) Average current clamp trace derived from 25 cells showing the response to a 2.5 s, 20 pA hyperpolarising current injection applied to cells at a prestimulus potential of -80 mV. (B) Voltage clamp protocol (top) and resultant average traces (bottom) of a series of 5 mV hyperpolarising steps from a holding potential of -55 mV. (C) Plot showing the change in membrane current between the first 60 ms (a) and the final 60 ms (b) of a voltage step to -125 mV. (D) Average I-V plot of the current response during the final 60 ms of a 5 s test pulse for series of 5 mV hyperpolarising voltage steps applied to 6 neurons held at -55 mV.

The incrementally growing depolarizing 500 ms current stimuli (Fig 7A) lead to AP firing in all Re neurones. A graph plotting the fraction of cells firing 1 AP or more versus the amplitude of the depolarizing stimulus is shown in Figure 9A, whereas Figure 9B summarizes the relationship between number of spikes elicited and current stimulus applied. The graph in Figure 9B does not provide any information about the temporal dynamics of AP production during the 500 ms current stimulus. This feature of excitability is illustrated in Figure 9C

which plots of mean instantaneous frequency versus spike interval for applied current stimuli ranging from 10 to 60 pA. We also gathered an additional dataset from a smaller group (n=25) of Re neurons using 2.5 second long current stimuli. An example recording and pooled data from the 30 and 60 pA stimuli are shown in Figure 9D. These recordings show that maintained lower frequency (8-20 Hz) firing following post-burst accommodation could continue for at least 2.5 seconds. In reality we believe this activity is ostensibly similar to the maintained firing observed at resting membrane potential in most Re neurons (Figure 1).

It is clear from Figures 9C and D that, on average, when Re neurons receive current injections sufficient to inducing fire they tend to generate an initial burst of AP around 115-145 Hz followed by accommodation to maintained spiking rates around 10-30 Hz. Although providing a useful and standard summary, data averaged in the way shown in Figure 9C do not reflect the full diversity of firing behaviours that we observed in our population of Re recordings. In particular the full spectrum of behaviours featured both highly bursty and regular spiking cellular responses to the same stimulus (Figure 10A). This diversity of firing patterns is illustrated in an alternative manner by the cell by cell data presented in Figure 10B. Here there relative timing of APs (relative to the first = black symbols) is shown for a 60 pA depolarizing stimulus. This plot confirms that many cells fire a prominent and very high frequency initial AP burst, whereas other cells lack this initial strong burst and fire more regularly throughout the applied stimulus (e.g Figure 10A(b)).

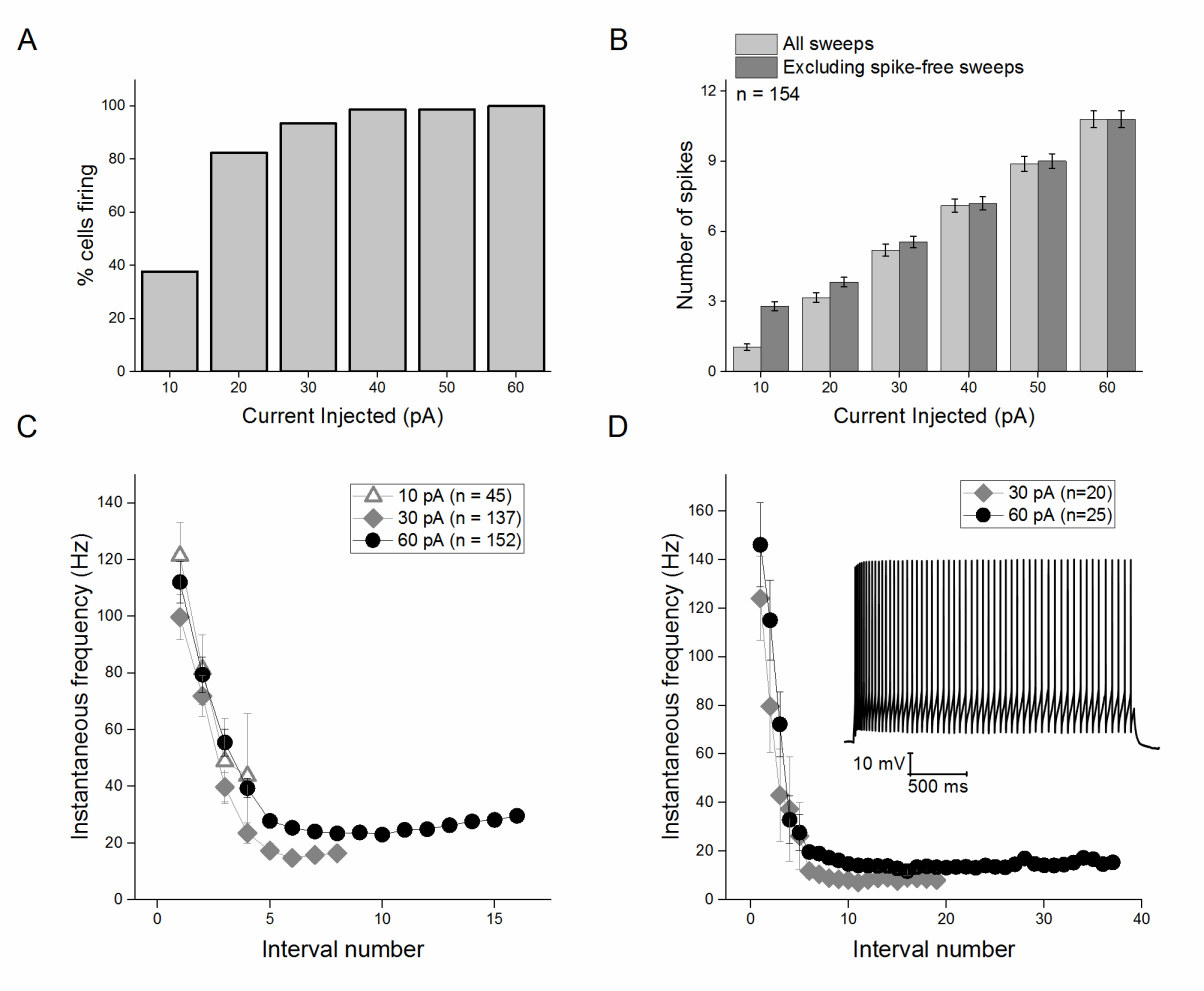

Figure 9. AP production in response to depolarising 500 ms "square-wave" current injections. (A) The fraction of cells generating at least one AP and **(B)** the mean number of AP produced in response to a series of 6 incremental 500 ms depolarising current injections (10 – 60 pA) from a set pre-stimulus potential of -80 mV. **(C)** A plot of instantaneous AP frequency vs interval number for a 10, 30 and 60 pA 500 ms current stimuli. (D) A plot of instantaneous AP frequency vs interval number and inset a sample voltage response, for a 30 and 60 pA 2.5 s current stimuli. All error bars represent SEM. All cells were set at -80 mV prior to current application.

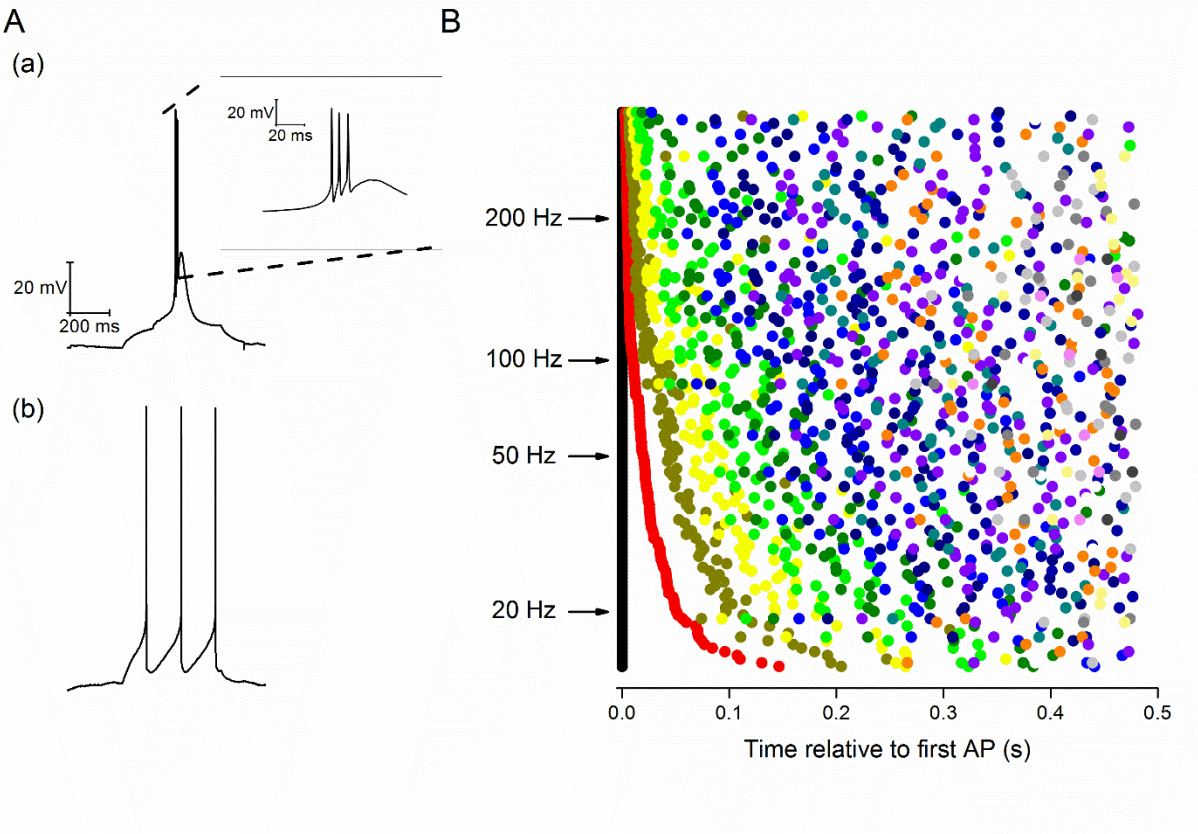

Figure 10. Diversity of firing following a depolarising current injection. (A) Sample voltage traces in response to a 10 pA 500 ms depolarising current injection from a set pre-stimulus membrane potential of -80 mV. Different neurons display diverse firing outcomes for this stimulus including (a) high frequency bursting and (b) regular firing. **(B)** Scatter plot displaying the heterogeneity of firing behaviour in response to a 60 pA depolarising current step. Each row represents a different neuron and the time at which the first AP is generated for each neuron is represented on the graph by a black point at 0 ms. The timing of all subsequent APs generated is plotted relative to the first spike. The second spike is represented by a red point, the third by dark yellow, the fourth by yellow and the fifth by green etc. Representing the data in this form illustrates the diverse array of different firing patterns present in the neuronal population.

In hippocampal pyramidal cells (Jensen *et al.*, 1996; Yue & Yaari, 2004; Brown & Randall, 2009) and some other “bursty” neurones, the presence of bursting correlates with the presence of a fast spike after-depolarizing potential (ADP). This afterpotential is best observed when very short (1-2 ms), strong current (1-2 nA) stimuli are used to elicit a single (primary) AP. In the period after the very brief current stimulus is removed the primary AP is followed by an ADP, which can, when sufficiently large, result in production of one or more

secondary APs. An ADP of this nature was present in many (67%) Re neurones. Examples of a subthreshold and a suprathreshold ADP are show in Figure 11, note the intense short burst of firing produced by the latter.

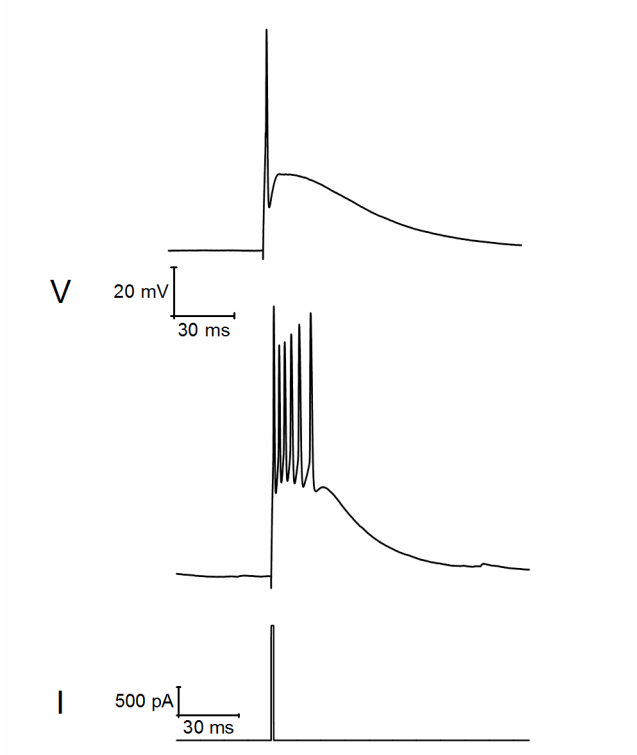

Figure 11. After-depolarising potential following a single spike. Two sample traces (top) of the voltage response following generation of a single spike elicited by a short (2 ms), strong (2 nA) square current injection (bottom).

High frequency firing driven by EPSP-like stimuli

Although “square-wave” current injections in current-clamp recordings are a very useful and standard means to characterise the excitability of neurons, they are not particularly representative of how cells are activated in vivo. To examine how physiological synaptic inputs might drive firing in Re neurons in vivo we used an approach in which current stimuli with EPSC-like waveforms (αEPSCs) were applied to Re neurons during current clamp recordings, an approach we have previously employed to study the basis of high frequency bursting in hippocampal CA3 pyramidal cells (Brown & Randall, 2009). To facilitate interpretation, and to parallel the datasets described above for conventional “rectangular” current stimuli (Figures 6,7,9,10,11), these stimuli were applied from a defined pre-stimulus

membrane potential of -80 mV, at which spontaneous firing is absent. We examined stimuli in which the decay rate of the injected current was varied across a 4-fold range (Figure 12), and also examined different stimulus peak amplitudes between 50 and 250 pA (Figure 13).

When sufficiently large (e.g 250 pA), αEPSC stimuli produced AP generation in 100% of Re neurons maintained at a pre-stimulus potential of -80 mV. In contrast, 50 pA stimuli almost always failed to produce APs (Figure 13B) and instead produced a subthreshold EPSP like waveform. With sufficiently large stimuli the αEPSC typically produced a high frequency (100-250 Hz) burst of 2 or more AP, as exemplified by Figure 12A. Furthermore as the decay of the αEPSC was slowed the mean spike output increased, approximately doubling as the decay time constant was lengthened from 5 to 20 ms.

A feature of the spiking response to αEPSC stimuli was that the action potential firing often occurred considerably after the peak of the injected current. Indeed, with just suprathreshold αEPSCs (i.e. 150 pA peak amplitude) and a 5 ms decay time constant the first AP occurred after the αEPSC waveform had decayed practically to baseline (Figure 13A and C). Even with the strongest αEPSC stimuli examined (250 pA) the first AP occurred some 5-12 ms after the peak of the current injection. In either case it was generally apparent that the αEPSC activated another subthreshold depolarizing current that in turn drove the cells towards their AP threshold.

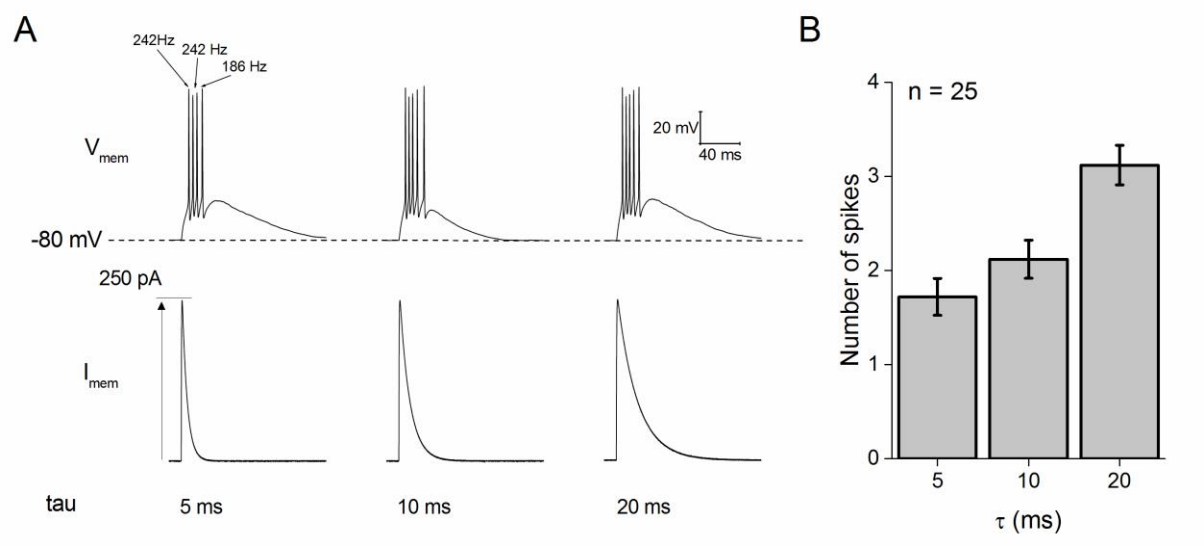

Figure 12. αEPSC current injections can elicit high frequency burst firing. (A) Sample voltage responses to 250 pA αEPSC current injections with time constants of 5, 10 and 20 pA, respectively. Note the resultant high frequency bursting observed in many cells. **(B)** A graph plotting the number of AP elicited versus the time constant of the αEPSC injected. As the time constant of the current injection increases so does the number of evoked APs.

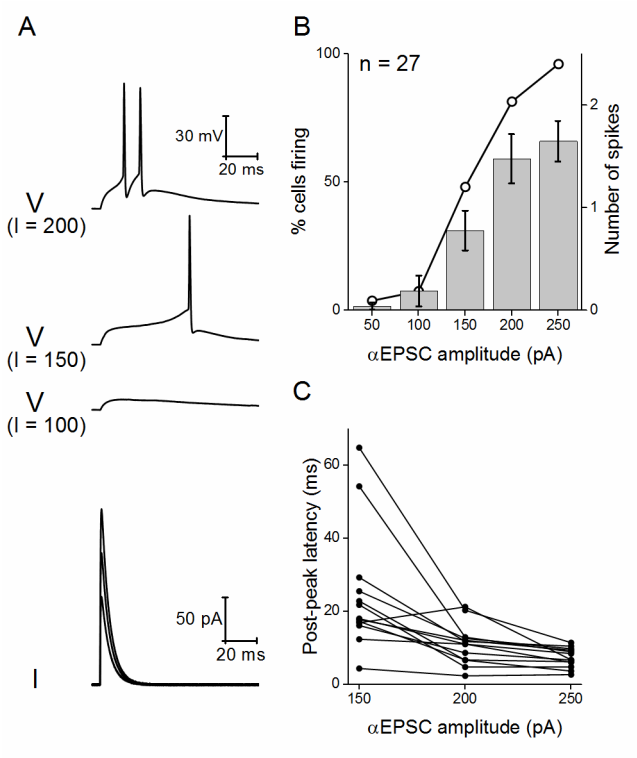

Figure 13. AP production in response to αEPSC current injections of varying sizes. (A) Sample voltage responses (top) to incrementally large αEPSC injections (tau_{decay} = 5 ms) ranging from 50-200 pA (bottom). **(B)** Graph plotting the mean number of spikes (column) and the percentage of neurons firing any spikes (line and symbol) in response to an αEPSC current injection with tau_{decay} = 5 ms. **(C)** A plot of the post-peak latency (i.e. the time after the peak of αEPSC the 1st AP fires) vs αEPSC amplitude (tau_{decay} = 5 ms).

Changes to excitability at more depolarized membrane potentials

The excitability data described above were collected from neurons placed at a set prestimulus membrane potential of -80 mV prior to delivery of a current stimulus. This level lies in the negative tail of the range of resting potentials seen in the Re population *in vitro* (Figure 1C). In a subset of cells we additionally collected datasets from a somewhat more depolarized pre-stimulus potential of -72 mV, although still one at which spontaneous spiking at rest was absent (Figure 14A). These recordings demonstrated that quite substantial changes in aspects of the excitability profile of Re neurons arose when their resting

potentials were changed by just a few mV. Perhaps somewhat surprisingly, depolarizing the pre-stimulus membrane potential by 8 mV had no effect on the total AP output observed during the 500 ms depolarizing current pulses of various amplitudes. Thus, very similar spike numbers were observed for each level of stimulus (Figure 14B) and the relationship between percentage of cells firing at least 1 AP and injected current was almost identical (Figure 14C). However, on visual examination of the voltage traces it was clear that the original high frequency AP burst seen in the majority of cells at -80 mV (Figures 9 & 10) was almost always absent in cells resting at -72 mV, as exemplified in Figure 14A. This is also reflected in the pooled data plotted in Figure 14D which present the mean instantaneous frequency for the first interspike interval elicited by each level of current injection. The initial spiking rate is around 5 to 8 times faster in the cells resting at -80 mV. In a similar vein, whereas 50-60% of cells at -80 mV produced a first spike pair with instantaneous frequency of 100-330 Hz, this was only around 5% for cells at -72 mV, and in this small population spiking did not exceed 155 Hz. The reason for the very similar total AP counts during the entirety of the 500 ms stimulus (Figure 14 B) was that the average rate of steady state spiking in the latter part of the current stimulus was approximately 10% higher in the cells starting from -72 mV.

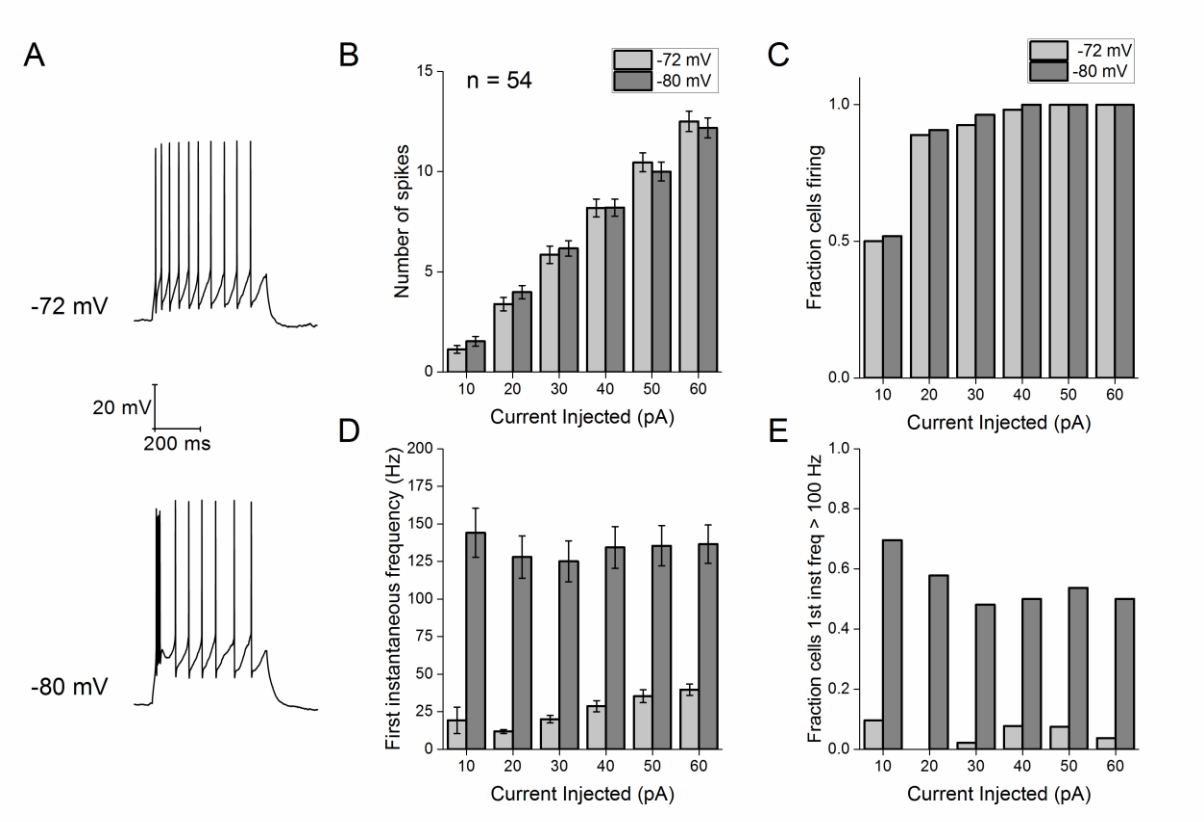

Figure 14. Firing behaviour in response to square current injections are dependent on membrane holding potential. (A) Sample voltage responses to a 60 pA square current

injection applied from pre-stimulus membrane potentials of -72 and -80 mV. **(B)** Graph showing the average number of spikes fired in response to 6 depolarising current injections (10-60 pA) from a Vm of -72 or -80 mV. Error bars represent SEM. **(C)** Graph showing the fraction of cells firing one or more AP for each current injection. Number of spikes fired or the fraction of cells firing in response to current injections were unaffected by Vm. **(D)** An illustration of the average instantaneous frequency between the first two spikes fired in response to a depolarizing stimulus of the indicated amplitude. **(E)** A graph showing the fraction of cells firing two action potentials at a frequency greater than 100 Hz. Both the average first instantaneous frequency and fraction of cells firing with a first instantaneous frequency >100 Hz were significant decreased by depolarising the membrane by 8 mV.

Electrophysiological and pharmacological evidence for a T-type Ca^{2+} conductance

The presence of both hyperpolarization-induced rebound firing in the absence of significant sag (Figures 7, 8), and the sub-threshold depolarizing potentials that trigger subsequent high frequency firing when Re neurons are depolarized from more negative potentials (Figures 9, 10, 12) are suggestive of the presence of T-type (CaV3 family) Ca^{2+} channels. Classically these channels have a low threshold for activation (more negative than AP threshold), and are readily inactivated when the resting potential becomes slightly depolarized (Perez-Reyes, 2003). Commensurate with this, the Allen Brain Atlas (http://mouse.brain-map.org) (Lein *et al.*, 2007) indicates robust expression of the CaV3.1 isoform of low threshold Ca^{2+} channel in Re. Furthermore, two previous studies (Graef *et al.*, 2009, 2011) have demonstrated expression of T-type Ca^{2+} channel mRNA and classical low threshold currents in the midline thalamus .

The size and geometrical complexity of CNS neurons in brain slices or in vivo, combined with their typically very large current densities can greatly hinder high fidelity voltage-clamp analysis of voltage-gated ionic conductances. However, with sufficient care and suitable protocols it is possible to gather some useful information particularly with regards to modest sized, slower-gating conductances, which suffer less from space-clamp associated issues. Voltage-clamp recordings were made pairing our standard pipette solution and our standard aCSF supplemented with 500 nM TTX (to eliminate voltage-gated sodium currents). Initially we applied an incremental series of voltage steps from a holding potential of -85 mV, this produced mixed currents like those presented in Figure 15A. Notably with modest depolarizations, for example to -63 mV, only inward currents were observed, whereas once the test potential became depolarized beyond about -45 mV large outward-going, partially inactivating currents began to dominate the response. These outward currents, which are carried by K^+ ions, rapidly increased in size to many nanoamps if depolarization was

increased further. The voltage-dependence and waveform kinetics of the inward current elicited with modest depolarizations was highly suggestive of a classical low threshold, T-type current. Using a series of small voltage steps separated by 2 mV increments we further profiled the inward current within the narrow voltage range where it was the predominate current. (Figure 15B). The current activated at the negative voltages expected for a T-type current and largely inactivated over around 60 ms of depolarization. We also gathered steady state inactivation data for these channels by varying the holding potential prior to an invariant step to -65 mV (Figure 15D) and profiled the rate of recovery from inactivation with a standard variable interval two step protocol (Figure 15E).

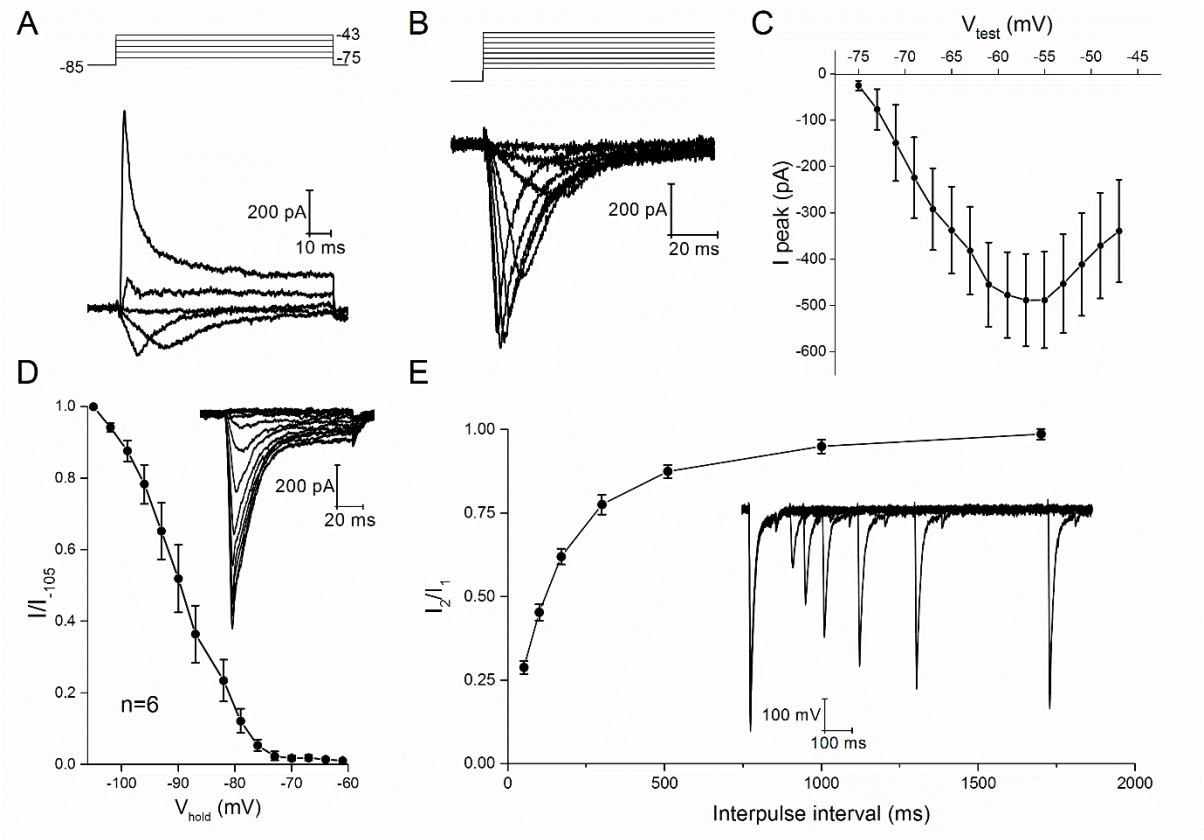

Figure 15. Gating properties of low-threshold inward currents. (A) Voltage-clamp protocol (top) and resultant current responses for a series of 8 mV incremental depolarising voltage steps applied from a holding potential of -85 mV. (B) Sample voltage trace and the subsequent current response to a series of 2 mV incremental depolarising voltage steps (from -75 – -47 mV) from a pre-stimulus holding potential of -85 mV. (C) Average I-V plot of the observed peak inward current in response to this series of 2 mV voltage steps. (D)

Inactivation curve showing the average voltage at which the T-type calcium current inactivates in Re neurons. (E) Line and symbol plot showing the rate of recovery from inactivation of T-type Ca^{2+} current determined with a standard variable interval two pulse protocol.

The pivotal neurophysiological roles of low threshold Ca^{2+} channels have been widely studied in other thalamic neurons for many years (Pape *et al.*, 2004), although the availability of reasonably potent and selective T-type channel blockers is a more recent advance (Xiang *et al.*, 2011). Application of one such molecule ML-218 (3 μM) caused a substantial decrease in the amplitude of the ADP elicited following a single short strong current injection (Figure 16A). The drug also reduced the instantaneous frequency of the first pair of spikes produced by a 500 ms depolarizing current step, without changing the total spike output from the stimulus. Finally, the drug eliminated the rebound firing produced when Re neurons resting at -70 mV (a membrane potential where 59% of neurons exhibit rebound firing following a hyperpolarising step) were hyperpolarized for 500 ms with a -50 pA current stimulus. The data in Figures 15 and 16 together indicate that T-type channels play a key role in the ability of Re neurones to produce very high frequency firing after transient sojourns at negative membrane potentials.

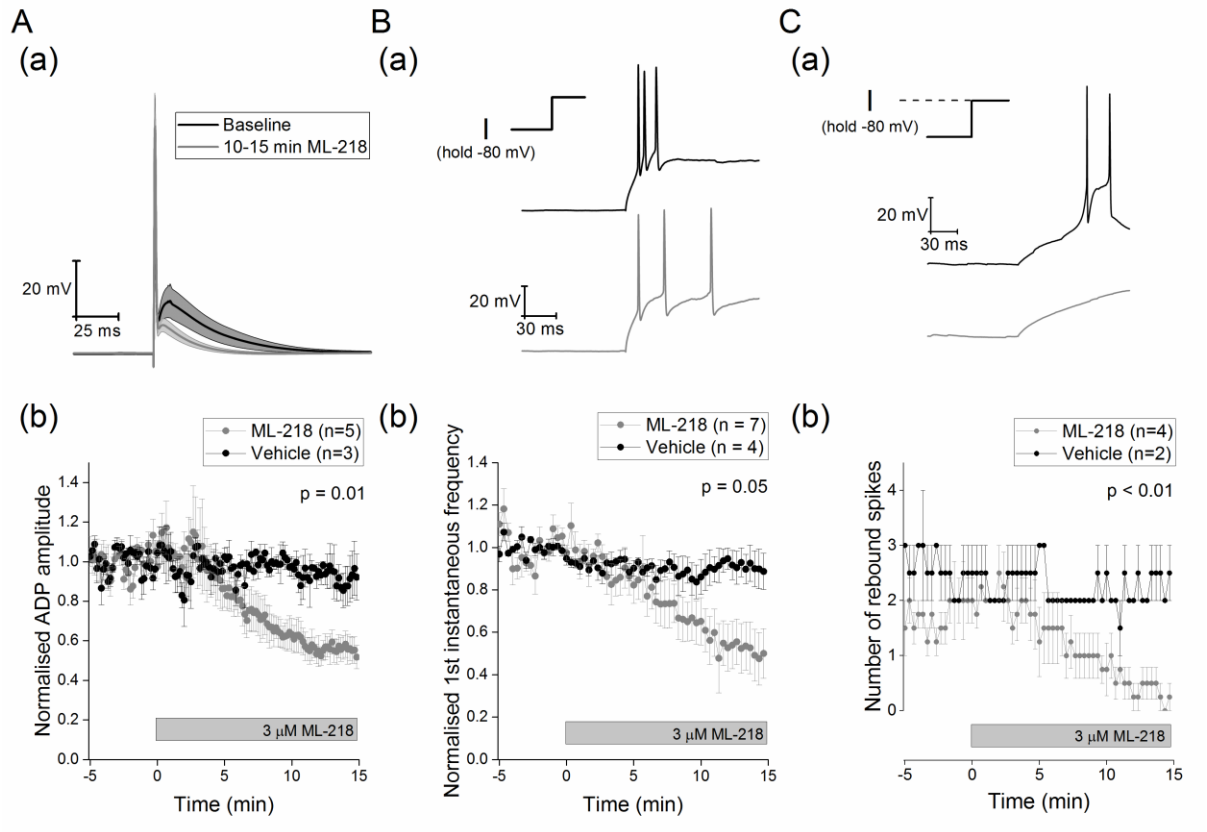

Fig 16. Pharmacological inhibition of T-type calcium channels alters firing properties. **(A)** Application of the T-type calcium blocker ML-218 (3 μM) reduces the amplitude of the ADP that arises following a single spike. (a) Average trace of the waveform of a single spike elicited by a short, strong current injection (2 ms, 2 nA) recorded during a 5 minute baseline (black), and during the last 5 minutes of a 15 minute exposure to 3 μM of T-type calcium channel blocker ML-218. Shaded area represents SEM. (b) A plot describing the time course of the effect of ML-218 on the average ADP amplitude normalised to the pre-drug baseline. **(B)** (a) Sample trace of the voltage response to a 100 pA depolarising current injection just prior to application of ML-218 (black) and following 15 minutes of exposure to ML-218 (grey). (b) A graph showing the effect of ML-218 on the first instantaneous frequency normalised to the predrug baseline. **(C)** (a) Sample traces showing the repolarisation driven rebound spiking following a -50 pA hyperpolarising current injection just prior to application of ML-218 (black) and following 15 minutes of exposure to ML-218 (grey). (b) A plot showing the effect of ML-218 on the average number of rebound spikes observed following repolarisation. All p values represent paired comparisons of the selected measurement between the pre-drug baseline and the final 5 minutes of the drug application.

Reduction in burstyness through activity-dependent intrinsic plasticity

The data in Figure 1-16 outline core aspects of the neurophysiology of rostral Re neurons, in particular their intrinsic excitability properties. Although often tonically firing at around 8 Hz at rest, after short periods at sufficiently negative potentials (i.e. ~-80 mV) the cells are capable of producing very high frequency burst firing, sometimes reaching instantaneous frequencies in excess of 300 Hz. The presence of an ML-218-sensitive, low threshold Ca^{2+} conductance seems central to the production of this high frequency burst firing. Intrinsic neuronal plasticity describes how the excitability properties of neurons can be modified by “experience” delivered experimentally as a conditioning stimulus of some form. For example, we have previously described how the burstyness of hippocampal pyramidal neurons can be persistently reduced either by brief cell-intrinsic activity patterns or via the activation of metabotropic glutamate receptors at synapses (Brown & Randall, 2009; Brown *et al.*, 2011).

We were curious if we could identify a similar means to transform the excitability of Re neurons. *In vivo*, the nucleus reuniens exhibits a strong theta oscillation and the firing of many neurons is synchronized to this (Jankowski *et al.*, 2014, 2015; Ito *et al.*, 2015). We therefore decided to employ a theta-paced burst firing protocol as a candidate conditioning stimulus for induction of intrinsic plasticity in Re neurons. Notably a similar protocol has

proved effective in persistently altering excitability of hippocampal neurons (Brown & Randall, 2009). In whole cell current clamp recordings we maintained the prestimulus membrane potential at -80 mV and collected a data sweep every 10 s. In all sweeps we first applied a 2 nA, 2ms stimulus to evoke a single spike and subsequent ADP (as in Figures 11 and 16A); notably we did not use cells in which the ADP triggered AP firing as this complicates quantification of this afterpotential and consequently experimental interpretation. In every second sweep the short-strong ADP eliciting stimulus was followed 1.5 s later by a 500 ms, 50 pA hyperpolarizing current pulse which could be used to measure passive properties (as in Figure 7B). We ran this protocol for at least 5 minutes to collect baseline data prior to applying the conditioning stimulus. The conditioning stimulus consisted of using short (2 ms) strong (2 nA) current injections to drive the cells to spike 5 times at 150 Hz (Figure 16A), this was repeated continuously every 200 ms for 15 s (thus a total of 75 bursts of 5 spikes in 15 s). During application of the conditioning stimulus we allowed the membrane potential to follow its desired trajectory rather than endeavouring to keep it at the fixed prestimulus level of -80 mV. Following application of the 15 s conditioning stimulus we returned to the stimulus protocol employed in the pre-conditioning period and followed the cell for a further 15 mins. In this post-conditioning period, as in the preconditioning period, the interstimulus membrane potential was again maintained at -80 mV.

As illustrated in Figure 17A and B, application of the 75 spike, theta-patterned conditioning protocol caused a progressive, acute change in the membrane potential of Re neurons. Thus, the cells on average hyperpolarized by over 6 mV, a change that followed an exponential trajectory that was largely complete after circa 9 theta burst cycles (i.e. 45 AP). Notably, this change did not stop the current stimuli from producing AP although the post-burst AHP was lost, likely as a result of the decreased driving force for K^+ ion fluxes that mediate the AHP. Notably this change was transient and cells returned to their pre-conditioning membrane potential within <1 min. In line with this the bias current used to keep the cells at -80 mV in the pre- and post-conditioning periods was not different.

More interestingly, following the conditioning stimulus a persistent change in the intrinsic excitability of Re neurons was observed. This was manifest as a decrease in the amplitude of the ADP observed following a single action potential (Figures 17C and D). Indeed, the ADP was largely absent in most cells and the amplitude measured was just that afforded by the need for the membrane to discharge (see Brown and Randall, 2009 for a discussion of this). The conditioning protocol acutely caused a 10-15% decrease in input resistance but this disappeared within 40 s no lasting changes to input resistance were observed. Thus, in the last 5 minutes on the experiment the input resistance was 100 ± 3% of its baseline value ($P>0.98$).

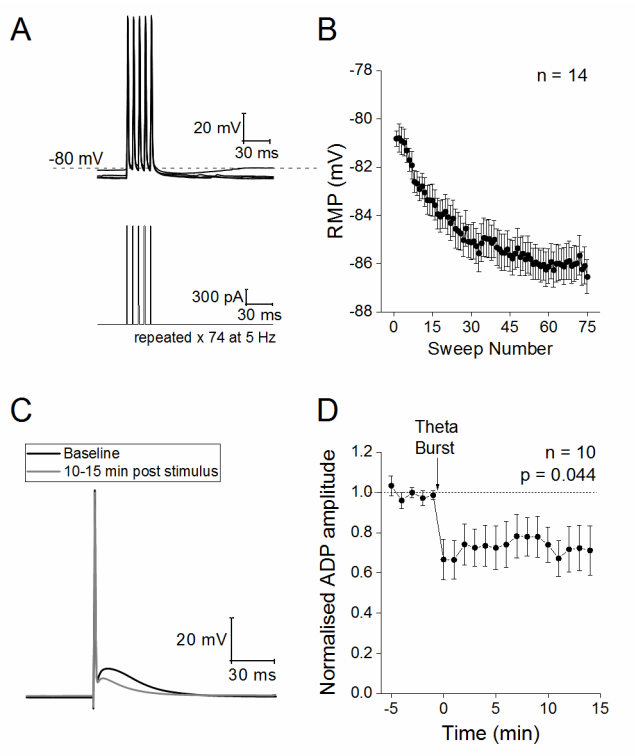

Fig 17. Re neurons exhibit intrinsic plasticity of the ADP (A) Sample voltage (top) and current (bottom) traces of a theta burst induction protocol used to induce intrinsic plasticity. Briefly each burst was driven induced with 5 short, strong (2 ms, 2 nA) current injections at a frequency of 150 Hz. 75 bursts were induced at 5 Hz in order to induce plasticity. (B) A plot showing the modest hyperpolarisation in the resting membrane potential that developed as the induction protocol progressed. (C) Voltage trace from an example experiment showing the average response to a single spike during the baseline period (black) and 10-15 minutes after the conditioning protocol(grey). (D) A plot showing the timecourse of the baseline-normalised ADP amplitude from 10 experiments.

Discussion

Thalamic neurons that project to the cortex, thalamocortical (TC) neurons, have been the subject of substantial neurophysiological investigation over the last 40 years. Amongst the most widely studied TC neurons are those which convey sensory information within either the visual or somatosensory systems, for example those whose cell bodies reside in the lateral geniculate and ventrobasal nuclei. Such studies have produced a general view of the intrinsic electrical properties of TC and how these shape the contribution of these neurons to network activities associated with sensory processing.

In this study we have characterized cell-level neurophysiological properties of Re neurons. Unlike classical TC neurons of sensory pathways, these cells of the midline thalamus receive little if any direct sensory information, but still both send and receive extensive cortical connections (Vertes et al 2015). We specifically focussed this work on neurons located in the rostral portion of Re because this is the predominant source of the afferent projections to the hippocampal and prefrontal circuits which have recently generated considerable interest (Varela *et al.*, 2014). Furthermore, from an anatomical perspective, rostral Re is also easy to identify unequivocally in murine brain slices. Although beyond the scope of this first study, in future it would be of interest to compare the properties of the rostral and caudal aspects of Re. Also given the diversity of intrinsic properties observed it would also be of interest to examine if there is a relationship between defined post synaptic target of these cells, established with retrograde labelling methods, and their neurophysiological properties at the cellular level.

Brain slice preparations encompassing the rostral nucleus reuniens are somewhat limiting for those wishing to examine the effects of pharmacological agents, especially in mice. This is because the region is both relatively small and resides on the midline, meaning each mouse provides only one slice (unlike, for example, the hippocampus or cerebellum where perhaps 10 unilateral slices can be obtained per animal). We stringently avoid recording from cells in slices that have been previously treated with a drug during a prior recording. Consequently, this typically limits pharmacological analysis to studying effects of one acute drug exposed cell per animal. Our only exception to this is studying cells in slices chronically treated with drugs to establish a particular background condition– for example, use of synaptic blockers throughout all recordings.

In whole cell recordings the majority of Re neurons were found to be relatively depolarized at rest. A major consequence of this was the presence of robust spontaneous firing of fast rising and decaying AP in the majority of cells. This firing often, although not always, occurred in a tonic fashion with a mean frequency around 8-9 Hz. These observations of spontaneous tonic firing in the majority of neurons are in agreement with Re recordings we have performed from slices obtained from both younger (6 weeks) and older mice (~1 year and ~2 years, unpublished data).

The depolarized resting potential and resultant spiking does not seem to arise as a consequence of entering the whole cell mode as spontaneous spiking was also clearly evident in loose patch or cell attached recordings in which the cytoplasmic contents are undisturbed. Furthermore, in our laboratory exactly the same recording solutions and conditions result in much more negative resting potentials in other neurons, for example both

CA1 and CA3 pyramidal cells (Brown & Randall, 2009; Booth *et al.*, 2016*b*) as well as various cortical neurons (Tamagnini *et al.*, 2014; Dawson *et al.*, 2015; Booth *et al.*, 2016*a*). Interestingly the depolarised membrane potential also contrasts starkly with the hyperpolarised membrane potential observed in both first and higher order thalamic nuclei (Jahnsen & Llinás, 1984; Varela & Sherman, 2007; Kolaj *et al.*, 2012). Indeed, to the best of our knowledge, in no other thalamic relay nuclei have the majority of neurons been reported to fire spontaneously when recorded during the light stage of a 12:12 day-night cycle. Although not supported by our loose patch/cell-attached observations, in which the cytoplasmic contents are undisturbed, we wondered if the depolarized resting potential seen may have reflected the relatively depolarized Cl^- equilibrium potential our intracellular solution produces combined with a significant level of tonic GABAergic drive. We found, however, that blocking $GABA_A$ receptors with GABAzine produced little effect on either resting potential or firing behaviours. Furthermore, blocking $GABA_A$ receptors did not appear to result in substantial increases in overall network activity in the Re, whereas in hippocampus and many areas of cortex pharmacological elimination of ongoing GABAergic inhibition generally produces huge hypersynchronous epileptiform burst events (Brown *et al.*, 2003).

Although the properties of synaptic inputs to Re neurons are not a major feature of this study, which instead focusses on intrinsic properties, it is notable that Re cells receive a significant ongoing spontaneous synaptic barrage. Indeed, even when spontaneous firing of neurons throughout the slice was eliminated with TTX, Re neurones received a substantial barrage of spontaneous miniature synaptic input. The quantal sizes of many of these events measured in voltage clamp, combined with the relatively high input resistance of Re neurons would indicate that they are individually capable of transiently driving the membrane potential a few mV depolarized. A thorough study of the properties and plasticity of key defined synaptic input pathways to Re neurons is unquestionably required to better understand how this component of the higher order thalamus contributes to circuit function. Optogenetic approaches would seem highly suited to this objective. Having said this, our work reveals that blocking all spontaneous ionotropic, amino acid-mediated synaptic function had no discernible effect on the rates of spontaneous spiking or the distribution of resting potentials within the reduced complexity of a brain slice preparation.

The predominant spontaneous firing frequencies of Re neurons corresponds well with the mean firing rates of Re neurons described in vivo (Ito et al. 2015) as well as the robust theta rhythm that can be recorded *in vivo* with electrodes implanted into Re. Indeed, autocorrelations of *in vivo* extracellular recordings of the firing of single Re neurons also reveals a strong phase locking to theta rhythms (Jankowski et al. 2014). Importantly, in brain

slices, normal CNS circuit connectivity and resultant network activity is lost, consequently the observation of spontaneous firing at rates in the theta band suggest that Re could be an intrinsic theta generator and may in turn relay this activity to the limbic structures to which it is connected. The fact that we found many Re neurons fired tonically at ~8 Hz in blockers of glutamatergic and GABAergic synaptic transmission lends further support this concept of a theta range oscillator intrinsic to Re neurons. Full testing of the idea that Re can act as a theta generator will require in vivo experiments, for example using optogenetic or pharmacogenetic manipulation of Re neurons whilst recording network behaviours in Re and defined projection targets. One initial study of this nature indicates that theta activity in hippocampal area CA1 is preserved when Re is lesioned with ibotenic acid or firing rates are optogenetically reduced (Ito et al. 2015). This may be because the primary hippocampal targets of Re projections appears to be interneurons, rather than pyramidal cells (M. Craig and C McBain, personal communication).

Although able to intrinsically fire spikes tonically in the theta frequency range in the absence of synaptic drive, the spiking behaviour of Re neurons in vivo will unquestionably be modulated and modified by various forms of excitatory and inhibitory synaptic drive into these cells. These synaptic influences will arises from multiple sources (McKenna & Vertes, 2004), most notably various components of the limbic system. Synaptic inhibition is likely to pivotally involve input from the reticular nucleus of the thalamus and the zona incerta (Cassel *et al.*, 2013)(Cholvin *et al.*, 2013)l. As outlined above, for those wishing to understand Re contribution to CNS circuits the functional properties of these afferent inputs to Re are worthy of much more experimental consideration in the future.

Compared to the cortical and hippocampal principal cells we have recorded *in vitro* using similar solutions at similar temperatures, Re neurons have a much higher input resistance. Hence, the average value in this study was over 600 MΩ, whereas we find, for example, adult CA1 pyramidal cells are typically circa 130 MΩ, pyramidal cells in layer 2 of perirhinal cortex average 100 MΩ (Tamagnini *et al.*, 2014) and layer 2/3 stellate cells in the dorsal end of entorhinal cortex average 40 MΩ (Booth *et al.*, 2016). To some extent their high input resistance likely reflects the smaller size of Re neurons (capacitance circa. 50% lower), but also points to a relative paucity of active background K^+ channels. Rodent TC neurons in other nuclei recorded with broadly similar methods (patch clamp in slices, ~32-35 C, Kgluconate pipette solution) typically have an input resistance of ~200 MΩ and resting potentials around -60 to -70 mV. It is notable, however, we have been unable to find any methodologically equivalent (i.e. patch clamp at circa 33°C with Kgluconate intracellular solution) studies of other thalamic nuclei at the same adult age as our mice (circa 4 months).

Iindeed, many TC neuron studies employ much younger rodents often <=3-4 weeks of age. Cells in such animals might be expected to have higher input resistances than those of trua adults as this feature of membrane physiology generally decreases with age.

A paucity of active background K^+ channels is also is a likely contributor to the depolarized resting potential of Re neurons compared to various cortical and hippocampal pyramidal cells studied under identical conditions. The combination of depolarized resting potentials and high input resistances found in Re neurons mean subthreshold cells need little depolarizing current to initiate firing. For example, even when set at -80 mV, around the 95% percentile of resting potentials, only 20 pA of current is required to bring around 80% of the cells to firing threshold (Figures 6 and 9). The large input resistance of Re cells also means they have a comparatively long membrane time constant averaging almost 40 ms. This means voltage changes in either direction are relatively slow. This maybe particularly pertinent for shaping the decay of synaptic potentials and also spike after-potentials. For example, the timecourse over which the AHP declines seems to pace firing at rest and anything which reduced input resistance without causing substantial hyperpolarization could speed firing. This could potentially occur, for example, through a GABAergic shunting conductance if the chloride equilibrium potential was not too negative. Additional studies utilizing gramicidin-perforated patch or dynamic clamp could be very informative in this regard.

The Ih current and the sag it produces in voltage recordings is a cardinal feature of other TC neurons. This conductance plays a role in determination of resting potential and its gating has long been considered crucial to facilitate transitions between hyperpolarised potentials where burst firing predominates and more depolarised modes of tonic firing. It is also considered crucial to the emergence of rhythmic activities in the thalamus (McCormick & Pape, 1990; Pape, 1996). Notably Re neurons appear to lack entirely hyperpolarization-activated sag and Ih-like currents (Figures 7B and 8), although these exact same recording conditions are capable of supporting robust Ih-mediated currents in other cells types (Booth et al 2016a and 2016b). The absence of Ih-like currents and sag is also in line with the relative lack of HCN channel expression in Re as reported in the Allen brain atlas (www.mouse.brain-map.org).

In contrast to other TC cells, the lack of Ih and associated sag in Re neurons means other mechanisms must account for their depolarised resting membrane potential.. It seems likely, the lack of Ih could produce telling consequences for how Re neurons contribute to their cognitive networks, and suggest substantial differences from the behaviours of other more widely studied TC neurons.

Some degree of diversity was seen in the patterns of spontaneous firing in the Re. Unquestionably most cells fired in a tonic fashion at 2-16 Hz, although more intermittent or bursty patterns of firing were seen in a minority of cells. Notably, the only cells which spontaneously fired high frequency spike bursts where those with very negative mean resting potentials. In these cells, the occasional spontaneous bursts of spikes which could exceed instantaneous frequencies of 200 Hz, were seen atop an initiating depolarizing transient, which based on others observation here, likely reflects a burst of feedforward activation of low threshold Ca^{2+} channels.

To investigate the intrinsic properties underlying the neurophysiological profile of Re neurons we extended our studies to look at how various current stimuli triggered AP production. In this work to reduce the variability that arises from cell to cell difference in resting potential we initially set the prestimulus resting potential to -80 mV, since at this negative level there is no on-going spontaneous firing which also simplifies interpretation of data. From this hyperpolarized prestimulus membrane potential sufficiently large depolarizing current injections produced firing. For over 80% of cells only 20 pA of applied current was required to produce spiking. In many cells the first 2-4 spikes arrived in the form of an initial high frequency spike burst, such that the mean instantaneous frequency of the first spike pair was around 120 Hz (Figures 9, 10 & 14)- although observations in excess of 200 Hz were not uncommon. This was the case with either the weakest or strongest suprathreshold stimuli (Figures 9 and 10). Indeed, with the weaker current stimuli, often only an initial high frequency burst of spiking was observed (Figures 7A & 9C), whereas with stronger stimuli, for example 30 or 60 pA, the initial burst was typically followed by more tonic spiking at 20-30 Hz (Figures 9 and 10). This behaviour is typical of TC neurons however Figure 10 highlights the variety of responses we observed. The initial frequency of firing of a Re neuron correlates significantly with the size of its observed ADP ($r=0.62$, $p<0.001$) suggesting that the variable expression of T-type calcium channels in these neurons could be responsible for the observed diversity. Neurons in the Re have been classified into 4 groups based on the differential expression of Ca^{2+} binding proteins calbindin and calretinin (Bokor *et al.*, 2002). As such it also seems plausible that differential calcium buffering capabilities between groups could contribute to the observed diversity. Given that the Re appears to be first thalamic nucleus in which such variety of responses from a fixed potential has been reported, future studies should focus on the underlying cellular mechanisms responsible.

High frequency burst spiking was also notable when cells at -80 mV were activated with short (2 ms) strong (1-2 nA) current stimuli that rapidly elicited a single primary AP (Figure 11) or αEPSC current stimuli (Figures 12 & 13). In these cases the spike burst occurred after

the current stimulus was over, indicating that pro-spiking neurophysiological processes initiated during the current stimulus continued. These processes were apparent in the ADP that followed the single spike driven by short strong current injections (Figure 11) or the deviations from a typical EPSP waveform in the αEPSC-driven burst firing (Figures 12 & 13).

The high-frequency burst firing in response to 500 ms depolarizing stimuli was eliminated when the Re cells where placed at -72 mV prior to application of the current stimulus. At this potential, the low threshold inward current with classical T-type channel biophysics seen in voltage-clamped Re neurons is essentially completely inactivated, whereas at -80 mV some 15% of the channels appear available (Figure 15D). In line with this, high frequency bursting driven by depolarizing current stimuli, both short strong (Figure 16A) and longer and weaker (Figure 16B) as well as from an "anodal break" following hyperpolarization are also attenuated by the selective T-type blocker ML-218.

Thus, Re neurons exhibit radically different firing outputs to depolarizing stimuli depending on their membrane potential prior to the arrival of the stimulus. A shift of only 8 mV completely reconfigures the resultant spiking response. This appears to be predominantly due to the presence of low threshold, T-type Ca^{2+} channels. The currents arising from these voltage-gated channels have long be shown to play a prominent role in the neurophysiological profile of various thalamic neurons, in particular those of the reticular nucleus and the lateral geniculate. Furthermore, two of the very few prior papers employing cellular recordings in the midline thalamic nuclei have focussed on T-type channels and their modulation in rodent models of epilepsy and alcoholism (Graef *et al.*, 2009, 2011). T-type Ca^{2+} channels are effectively activated by EPSP-like waveforms (Warre *et al.*, 2002), and T-type currents have been shown to contribute to the depolarizing envelope of EPSPs in cerebellar Purkinje cells (Ly *et al.*, 2016).

The ability of Re neurons to fire short bursts of AP at very high frequencies either in response to depolarizing current stimuli or through "rebound" following a negative current stimulus is important when considering consequences for the synapses these cells form in the hippocampus, prefrontal cortex and elsewhere. Due to the effects of short-term synaptic plasticity, the glutamatergic drive generated from a Re afferent pathway exhibiting occasional bursts of spikes at 100-300 Hz will certainly be very different from that produced by tonic 8 Hz firing. Notably, nothing is known about the short-term plasticity of Re projections and related features of synaptic function such as their probability of release and post-synaptic response kinetics.

The synaptic terminations of Re projections into area CA1 of the hippocampus are concentrated in the *stratum lacunosum moleculare*, which is also where most temporoammonic inputs from the entorhinal cortex terminate. In this distal dendritic region far from the CA1 pyramidal cell layer, electrical stimulation of axons with small numbers of high frequency bursts produces robust long-term potentiation of excitatory synapses on hippocampal neurons (Remondes & Schuman, 2003; Booth *et al.*, 2014, 2016*b*). Although this long-term synaptic plasticity is frequently attributed to temporoammonic afferents, unquestionably a component of such responses arise from stimulation of Re neurons which have long been known to produce a robust synaptic response in area CA1 (Dolleman-Van der Weel *et al.*, 1997; Dolleman-Van der Weel & Witter, 2000) and also to exhibit robust LTP (Bertram & Zhang, 1999). On this basis, high frequency burst firing of presynaptic Re neurons would seem ideal to drive synaptic potentiation of their inputs to the hippocampus.

Importantly, our data suggest the means through which Re neurons will communicate with their downstream synaptic partners will depend strongly on their resting potential. Cells around -65 mV may be tonically firing in the theta frequency range. Assuming these spikes generated in the perisomatic region successfully complete their journey to downstream synapses, post-synaptic responses will be produced every so often, largely dependent on probability of release. One would probably not expect much in the way of EPSP summation or short-term synaptic plasticity. Re neurons resting more depolarized than -72 mV but not spontaneously firing will not produce high frequency spike bursts when activated, for example by excitatory synaptic drive, and thus may only produce single spikes or a period of low frequency regular spiking. In contrast Re cells sat at -80 mV or below will likely generate a robust multispike burst on activation that could drive a substantial summated, frequency facilitated EPSP in post-synaptic cells, a response of the sort that might induce synaptic plasticity if repeated a few times. Notably, Re cells do not need to spend long at negative potentials for T-type channels to deinactivate and the ability to generate high frequency spike bursts to emerge. For example 300 ms at -85 mV deinactivates ~80% of T-type channels (Figure 15 E).

For the reasons described above, both gaining an understanding of the actual membrane potentials of Re neurons in vivo and determining key things that control membrane potential are crucial to understanding how Re contributes to the function of CNS circuits in which it sits. For example, metabotropic receptor-mediated IPSPs (produced by activation of GABAB, dopamine D2 or noradrenaline $\alpha 2$ receptors, coupled to GIRK K^+ channels) last at least 500 ms and can often last many seconds (see North & Surprenant, 1985 for example), certainly enough time to deinactivate T-type channels and enable burst firing. Notably Re

receives inputs from the ventral tegmental area and the locus coeruleus (Cassel *et al.*, 2013) and there are correlations between expression of α2 receptors in Re and behaviour (Wilmot *et al.*, 1988)

In vitro electrophysiological recordings are generally performed with the expectation, or at least hope, that the recorded neurophysiological outcomes relate to those of the corresponding cells *in vivo*. With faith in this expectation, it is possible to use the data obtained *in vitro* to consider how the neurophysiological properties of the investigated cell shape its functional contributions the various neural circuits of which it forms part. Such interpretations can be performed at various levels, from the sorts of general ideas voiced here to utilization of the data to aid in the building of computational models. By performing the first substantial cellular level study of Re neurones, our goal here has been to obtain insights of this nature; and accordingly we have discussed some of the ways the properties we have observed in vitro may shape the behaviour of Re neurons in CNS circuits. Furthermore, based on our data, we are also currently starting to build mathematical models of Re neurons.

We feel, however, it is prudent to introduce a note of caution; it is certainly possible that the cellular properties we have documented are not facsimiles of what would be seen with cellular recordings performed in vivo. Indeed, as we have discussed before (Brown and Randall 2009), the very process of preparing brain slices could induce significant and long-lasting changes to intrinsic and/or synaptic neurophysiological features of a neuron. However, the task of obtaining over 100 *in vivo* patch clamp (or intracellular) recordings from a deep and relatively small midline structure in the murine brain would be daunting, and if data gathered without the confounds of anaesthesia were required (for example from head-fixed recordings), the challenge might best be described as Herculean.

Consequently, in the absence of equivalent *in vivo* data we feel this dataset is valuable for those who wish to better understand the contribution of Re to various CNS processes, particularly so when considered hand in hand with what we have learnt from recent *in vivo* investigations of the activity of these neurons in behaving rodents (Jankowski *et al.*, 2014, 2015; Ito *et al.*, 2015) as well as studies that outline changes to Re neurons in disease models (Graef *et al.*, 2009, 2011).

References

Aggleton JP (2014). Looking beyond the hippocampus: old and new neurological targets for

understanding memory disorders. *Proc Biol Sci*; DOI: 10.1098/rspb.2014.0565.

Bertram EH & Zhang DX (1999). Thalamic excitation of hippocampal CA1 neurons: a comparison with the effects of CA3 stimulation. *Neuroscience* **92,** 15–26.

Bokor H, Csáki A, Kocsis K & Kiss J (2002). Cellular architecture of the nucleus reuniens thalami and its putative aspartatergic/glutamatergic projection to the hippocampus and medial septum in the rat. *Eur J Neurosci* **16,** 1227–1239.

Booth CA, Brown JT & Randall AD (2014). Neurophysiological modification of CA1 pyramidal neurons in a transgenic mouse expressing a truncated form of disrupted-in-schizophrenia 1. *Eur J Neurosci* **39,** 1074–1090.

Booth CA, Ridler T, Murray TK, Ward MA, de Groot E, Goodfellow M, Phillips KG, Randall AD & Brown JT (2016*a*). Electrical and Network Neuronal Properties Are Preferentially Disrupted in Dorsal, But Not Ventral, Medial Entorhinal Cortex in a Mouse Model of Tauopathy. *J Neurosci* **36,** 312–324.

Booth CA, Witton J, Nowacki J, Tsaneva-Atanasova K, Jones MW, Randall AD & Brown JT (2016*b*). Altered Intrinsic Pyramidal Neuron Properties and Pathway-Specific Synaptic Dysfunction Underlie Aberrant Hippocampal Network Function in a Mouse Model of Tauopathy. *J Neurosci*.

Brown JT, Booth CA & Randall AD (2011). Synaptic activation of mGluR1 generates persistent depression of a fast after-depolarizing potential in CA3 pyramidal neurons. *Eur J Neurosci* **33,** 879–889.

Brown JT, Gill CH, Farmer CE, Lanneau C, Randall AD, Pangalos MN, Collingridge GL & Davies CH (2003). Mechanisms contributing to the exacerbated epileptiform activity in hippocampal slices of GABAB1 receptor subunit knockout mice. *Epilepsy Res* **57,** 121–136.

Brown JT & Randall AD (2009). Activity-dependent depression of the spike after-depolarization generates long-lasting intrinsic plasticity in hippocampal CA3 pyramidal neurons. *J Physiol* **587,** 1265–1281.

Cassel J-C, Pereira de Vasconcelos A, Loureiro M, Cholvin T, Dalrymple-Alford JC & Vertes RP (2013). The reuniens and rhomboid nuclei: Neuroanatomy, electrophysiological characteristics and behavioral implications. *Prog Neurobiol* **111,** 34–52.

Ceolin L, Kantamneni S, Barker GRI, Hanna L, Murray L, Warburton EC, Robinson ESJ,

Monn JA, Fitzjohn SM, Collingridge GL, Bortolotto ZA & Lodge D (2011). Study of Novel Selective mGlu2 Agonist in the Temporo-Ammonic Input to CA1 Neurons Reveals Reduced mGlu2 Receptor Expression in a Wistar Substrain with an Anxiety-Like Phenotype. *J Neurosci* **31,** 6721–6731.

Cholvin T, Loureiro M, Cassel R, Cosquer B, Geiger K, De Sa Nogueira D, Raingard H, Robelin L, Kelche C, Pereira de Vasconcelos A & Cassel J-C (2013). The ventral midline thalamus contributes to strategy shifting in a memory task requiring both prefrontal cortical and hippocampal functions. *J Neurosci* **33,** 8772–8783.

Dawson N, Kurihara M, Thomson DM, Winchester CL, McVie A, Hedde JR, Randall AD, Shen S, Seymour PA, Hughes ZA, Dunlop J, Brown JT, Brandon NJ, Morris BJ & Pratt JA (2015). Altered functional brain network connectivity and glutamate system function in transgenic mice expressing truncated Disrupted-in-Schizophrenia 1. *Transl Psychiatry* **5,** e569.

Dolleman-Van der Weel MJ, Lopes da Silva FH & Witter MP (1997). Nucleus Reuniens Thalami Modulates Activity in Hippocampal Field CA1 through Excitatory and Inhibitory Mechanisms. *J Neurosci* **17,** 5640–5650.

Dolleman-Van der Weel MJ & Witter MP (2000). *Nucleus reuniens thalami innervates γ aminobutyric acid positive cells in hippocampal field CA1 of the rat*.

Giocomo LM & Hasselmo ME (2006). Difference in time course of modulation of synaptic transmission by group II versus group III metabotropic glutamate receptors in region CA1 of the hippocampus. *Hippocampus* **16,** 1004–1016.

Graef JD, Huitt TW, Nordskog BK, Hammarback JH & Godwin DW (2011). Disrupted thalamic T-type Ca2+ channel expression and function during ethanol exposure and withdrawal. *J Neurophysiol* **105,** 528–540.

Graef JD, Nordskog BK, Wiggins WF & Godwin DW (2009). An acquired channelopathy involving thalamic T-type Ca2+ channels after status epilepticus. *J Neurosci* **29,** 4430–4441.

Hallock HL, Wang A & Griffin AL (2016). Ventral Midline Thalamus Is Critical for Hippocampal-Prefrontal Synchrony and Spatial Working Memory. *J Neurosci* **36,** 8372–8389.

Hallock HL, Wang A, Shaw CL & Griffin AL (2013). Transient inactivation of the thalamic nucleus reuniens and rhomboid nucleus produces deficits of a working-memory

dependent tactile-visual conditional discrimination task. *Behav Neurosci* **127,** 860–866.

Ito HT, Zhang S-J, Witter MP, Moser EI & Moser M-B (2015). A prefrontal-thalamo-hippocampal circuit for goal-directed spatial navigation. *Nature* **522,** 50–55.

Jahnsen H & Llinás R (1984). Electrophysiological properties of guinea-pig thalamic neurones: an in vitro study. *J Physiol* **349,** 205–226.

Jankowski MM, Islam MN, Wright NF, Vann SD, Erichsen JT, Aggleton JP & O'Mara SM (2014). Nucleus reuniens of the thalamus contains head direction cells. *Elife*; DOI: 10.7554/eLife.03075.

Jankowski MM, Passecker J, Islam MN, Vann S, Erichsen JT, Aggleton JP & O'Mara SM (2015). Evidence for spatially-responsive neurons in the rostral thalamus. *Front Behav Neurosci* **9,** 256.

Jensen MS, Azouz R & Yaari Y (1996). Spike after-depolarization and burst generation in adult rat hippocampal CA1 pyramidal cells. *J Physiol*199–210.

Jones MW & Wilson MA (2005). Theta rhythms coordinate hippocampal-prefrontal interactions in a spatial memory task. *PLoS Biol* **3,** e402.

Kolaj M, Zhang L, Ronnekleiv OK & Renaud LP (2012). Midline thalamic paraventricular nucleus neurons display diurnal variation in resting membrane potentials, conductances, and firing patterns in vitro. *J Neurophysiol* **107,** 1835–1844.

Lein ES et al. (2007). Genome-wide atlas of gene expression in the adult mouse brain. *Nature* **445,** 168–176.

Ly R, Bouvier G, Szapiro G, Prosser HM, Randall AD, Kano M, Sakimura K, Isope P, Barbour B & Feltz A (2016). Contribution of postsynaptic T-type calcium channels to parallel fibre-Purkinje cell synaptic responses. *J Physiol* **594,** 915–936.

Mair WGP, Warrington EK & Weiskrantz L (1979). Memory disorder in korsakoff' s psychosis a neuropathological and neuropsychological investigation of two cases. *Brain* **102,** 749–783.

McCormick DA & Pape HC (1990). Properties of a hyperpolarization-activated cation current and its role in rhythmic oscillation in thalamic relay neurones. *J Physiol* **431,** 291–318.

McKenna JT & Vertes RP (2004). Afferent projections to nucleus reuniens of the thalamus. *J Comp Neurol* **480,** 115–142.

North RA & Surprenant A (1985). Inhibitory synaptic potentials resulting from alpha 2-adrenoceptor activation in guinea-pig submucous plexus neurones. *J Physiol* **358,** 17–33.

Pape H-C (1996). Queer Current and Pacemaker: The Hyperpolarization-Activated Cation Current in Neurons. *Annu Rev Physiol* **58,** 299–327.

Pape H-C, Munsch T & Budde T (2004). Novel vistas of calcium-mediated signalling in the thalamus. *Pflügers Arch Eur J Physiol* **448,** 131–138.

Perez-Reyes E (2003). Molecular physiology of low-voltage-activated t-type calcium channels. *Physiol Rev* **83,** 117–161.

Prasad JA & Chudasama Y (2013). Viral tracing identifies parallel disynaptic pathways to the hippocampus. *J Neurosci* **33,** 8494–8503.

Remondes M & Schuman EM (2003). Molecular mechanisms contributing to long-lasting synaptic plasticity at the temporoammonic-CA1 synapse. *Learn Mem* **10,** 247–252.

Santoro B, Chen S, Luthi A, Pavlidis P, Shumyatsky GP, Tibbs GR & Siegelbaum SA (2000). Molecular and functional heterogeneity of hyperpolarization-activated pacemaker channels in the mouse CNS. *J Neurosci* **20,** 5264–5275.

Sargolini F, Fyhn M, Hafting T, McNaughton BL, Witter MP, Moser M-B & Moser EI (2006). Conjunctive representation of position, direction, and velocity in entorhinal cortex. *Science* **312,** 758–762.

Tamagnini F, Scullion S, Brown JT & Randall AD (2014). Low concentrations of the solvent dimethyl sulphoxide alter intrinsic excitability properties of cortical and hippocampal pyramidal cells. *PLoS One* **9,** e92557.

Taube JS, Muller RU & Ranck JB (1990). Head-direction cells recorded from the postsubiculum in freely moving rats. I. Description and quantitative analysis. *J Neurosci* **10,** 420–435.

Varela C, Kumar S, Yang JY & Wilson MA (2014). Anatomical substrates for direct interactions between hippocampus, medial prefrontal cortex, and the thalamic nucleus reuniens. *Brain Struct Funct* **219,** 911–929.

Varela C & Sherman SM (2007). Differences in Response to Muscarinic Activation Between First and Higher Order Thalamic Relays. *J Neurophysiol* **98,** 3538–3547.

Vertes RP (2006). Interactions among the medial prefrontal cortex, hippocampus and midline thalamus in emotional and cognitive processing in the rat. *Neuroscience* **142,** 1–20.

Vertes RP, Hoover WB, Szigeti-Buck K & Leranth C (2007). Nucleus reuniens of the midline thalamus: link between the medial prefrontal cortex and the hippocampus. *Brain Res Bull* **71,** 601–609.

Vertes RP, Linley SB & Hoover WB (2015). Limbic circuitry of the midline thalamus. *Neurosci Biobehav Rev*; DOI: 10.1016/j.neubiorev.2015.01.014.

Warre RC., McNaughton NC. & Randall A. (2002). Differential discrimination of fast and slow synaptic waveforms by two low-voltage-activated calcium channels. *Neuroscience* **110,** 375–388.

Wilmot CA, Sullivan AC & Levin BE (1988). *Effects of diet and obesity on brain α1- and α2-noradrenergic receptors in the rat*.

Xiang Z et al. (2011). The Discovery and Characterization of ML218: A Novel, Centrally Active T-Type Calcium Channel Inhibitor with Robust Effects in STN Neurons and in a Rodent Model of Parkinson's Disease. *ACS Chem Neurosci* **2,** 730–742.

Xu W & Südhof TC (2013). A neural circuit for memory specificity and generalization. *Science* **339,** 1290–1295.

Yue C & Yaari Y (2004). KCNQ/M Channels Control Spike Afterdepolarization and Burst Generation in Hippocampal Neurons. *J Neurosci* **24,** 4614–4624.

Funding: Grant sponsor: Eli Lilly and Company and the University of Exeter.

Additional information section:

Conflict of interest statement: The authors declare that this work was completed with the absence of any conflicting interests, financial or otherwise.

Author contributions:

DW- conception and design of experiments, collection assembly analysis and interpretation of data. Drafting the article and critically revising it for critical intellectual content.JB- conception and design of experiments, collection assembly analysis and interpretation of data. Drafting the article and critically revising it for critical intellectual content.

AR- conception and design of experiments, collection assembly analysis and interpretation of data. Drafting the article and critically revising it for critical intellectual content.

Funding: This research was supported by a PhD studentship to DW co-supported by Eli Lilly and Company and the University of Exeter.

Acknowledgements: The authors wish to thank Hannah Smithers who provided some of the brain slices used in these studies because she was better at getting out of bed the DW.